Macromolecular Bioscience
www.mbs-journal.de

Harnessing Macromolecular Chemistry to Design Hydrogel Micro- and Macro-Environments

*Bram G. Soliman, Alessia Longoni, Gretel S. Major, Gabriella C. J. Lindberg, Yu Suk Choi, Yu Shrike Zhang, Tim B.F. Woodfield, and Khoon S. Lim**

Cell encapsulation within three-dimensional hydrogels is a promising approach to mimic tissues. However, true biomimicry of the intricate microenvironment, biophysical and biochemical gradients, and the macroscale hierarchical spatial organizations of native tissues is an unmet challenge within tissue engineering. This review provides an overview of the macromolecular chemistries that have been applied toward the design of cell-friendly hydrogels, as well as their application toward controlling biophysical and biochemical bulk and gradient properties of the microenvironment. Furthermore, biofabrication technologies provide the opportunity to simultaneously replicate macroscale features of native tissues. Biofabrication strategies are reviewed in detail with a particular focus on the compatibility of these strategies with the current macromolecular toolkit described for hydrogel design and the challenges associated with their clinical translation. This review identifies that the convergence of the ever-expanding macromolecular toolkit and technological advancements within the field of biofabrication, along with an improved biological understanding, represents a promising strategy toward the successful tissue regeneration.

1. Introduction

The concept of tissue engineering was first coined in 1970 to describe the research field focused on recapitulating the complexity of native tissues for therapeutic purposes by combining cells, biomaterials and biological stimuli.[1] Since then, there has been an overwhelming focus on identifying the ideal combination of these three elements to engineer functional tissues analogues. It is now appreciated that the intrinsic properties of the native cellular microenvironment (i.e., physico-chemical properties and architecture) play a crucial role in guiding cellular behavior.[2–4] This has driven the development of strategies to engineer three-dimensional (3D) microenvironments with characteristics similar to physiological in vivo environments, in order to influence biological responses such as cell migration, proliferation and differentiation.[3, 5]

A promising approach to direct cell fate is tailoring the properties of biomaterials to mimic specific characteristics

B. G. Soliman
School of Materials Science and Engineering
University of New South Wales
Sydney 2052, Australia

A. Longoni
Department of Orthopedics
University Medical Center Utrecht
Utrecht 3584CX, The Netherlands

G. S. Major, T. B. Woodfield, K. S. Lim
Department of Orthopedic Surgery and Musculoskeletal Medicine
University of Otago
Christchurch 8011, New Zealand
E-mail: khoon.lim@sydney.edu.au

G. C. J. Lindberg
Phil and Penny Knight Campus for Accelerating Scientific Impact
Department of Bioengineering
University of Oregon
Eugene, OR 97403, USA

Y. S. Choi
School of Human Sciences
The University of Western Australia
Perth 6009, Australia

Y. S. Zhang
Division of Engineering in Medicine
Department of Medicine
Brigham and Women's Hospital
Harvard Medical School
Cambridge, MA 02115, USA

K. S. Lim
School of Medical Sciences
University of Sydney
Sydney 2006, Australia

K. S. Lim
Charles Perkins Centre
University of Sydney
Sydney 2006, Australia

The ORCID identification number(s) for the author(s) of this article can be found under https://doi.org/10.1002/mabi.202300457

DOI: 10.1002/mabi.202300457

of native tissues. Among the different biomaterials used for tissue engineering applications, hydrogels have attracted considerable attention to fabricate biomimetic constructs.[3] Hydrogels are highly hydrated, 3D networks of cross-linked hydrophilic polymers.[3,6,7] Owing to their high-water content, they naturally resemble the native extracellular matrix (ECM) better than other polymeric biomaterials.[3,6] As the network is permeable for oxygen, nutrients and other water-soluble metabolites, hydrogels are particularly appealing for the encapsulation of a range of different cell types.[3,8–11] Hydrogels are tuneable and relatively easy to functionalize, offering great spatiotemporal control over their chemical, mechanical and biological properties.[3] The hydrogel microenvironment is defined by 1) the chemical structure and properties of the polymer(s) chosen for the 3D network, by 2) the type of crosslink used to form the polymer network (i.e., collectively termed macromolecular chemistry), and by 3) the presence of any additional bioactive components. The optimization of these parameters through rational design of the hydrogel and its macromolecular chemistry enables fabrication of hydrogels with a wide range of design features, permitting the fabrication of diverse and complex microenvironments.[3] For instance, hydrogel platforms with different characteristics have been successfully employed to guide encapsulated cells to form a variety of tissues including, cartilage,[8,12] bone,[9,13,14] vasculature,[10,14,15] innervation,[11,16] liver and heart.[3,17,18]

The aim of this review is to specifically highlight how macromolecular chemistry can be employed as a tool to design hydrogels with specific biomimetic properties that guide cell behavior. It is imperative to understand the hydrogel's design criteria imposed by the native microenvironment. As microenvironmental features vary across different organs, the native microenvironments of a range of human tissues are initially described. Factors that define the macromolecular chemistry of hydrogels and how they can be exploited to meet the design criteria of these microenvironments are reviewed, and then the relevant interplay between microscopic and macroscopic environmental features in shaping a cell-instructive tissue substitutes is discussed. Finally, biofabrication technologies used to include both micro- and macroscale cues in engineered tissue substitutes are reviewed, followed by a future outlook and translational perspective of rational hydrogel design in guiding tissue regeneration.

2. Microenvironmental Features of Native Tissues

Native tissues are defined by their 3D hierarchical spatial organization that result in unique tissue properties and permit them to execute high-order functional roles within the body.[5,13,19] Understanding the role of stimuli in native tissue physiology and during tissue healing provides crucial information for the design of ad hoc regenerative strategies. To that effect, a plethora of biochemical and physical cues that are critical to replicate the native tissue physiology and homeostasis when engineering hydrogel-based tissue substitutes. The heterogeneity that is inherent to native tissues is exemplified by highlighting the variation in biochemical and biophysical cues within bone, cartilage, and vascular tissues (**Table 1**).

2.1. Biochemical Cues

Tissue development, homeostasis, and healing after injury, are processes which are all orchestrated by specific biochemical cues present in the tissue ECM, and which guide cell behavior.[27–29] These biochemical cues can be of organic or inorganic origin, and can be conjugated to ECM macromolecules or present as soluble cues.[27,30] Growth factors are the most well-known class of biochemical cues which can influence a variety of cellular processes, including cell survival, proliferation, migration, differentiation and multicellular morphogenesis during development, injury, regeneration and aging.[31] These molecules are key regulators of cell-to-cell communication and can be secreted by cells and either present in soluble forms within the microenvironment, or sequestered among ECM proteins including glycoproteins such as fibronectin, fibrous proteins such as collagen and glycosaminoglycans (GAGs) such as heparan sulfate.[31,32] As a reflection of the precise spatial organization of cells within native tissues, biochemical cues are often compartmentalized in specific areas, creating tightly localized gradients.[33,34] For example, within the cartilage growth plate, chondrocytes in different areas express diverse levels of bone morphogenic protein (BMP) type 2 (BMP-2) and type 6 (BMP-6), creating a feedback cycle that regulates their proliferation and differentiation.[33,34] The spatial compartmentalization of biochemical cues is also essential for processes like angiogenesis. Vascular endothelial growth factor (VEGF), a growth factor that is secreted in response to increases in hypoxia within the tissue microenvironment, plays a major role in guiding angiogenic sprouting.[35–37] In response to VEGF secretion, nascent sprouts can be observed in neighboring capillaries that progress toward the hypoxic site by adopting a tip or stalk phenotype.[38] Notably, growth factor presentation in native tissues is dynamic with marked temporal changes in growth factor concentrations. For example, in response to bone injuries (e.g., fractures), BMP-2 levels in the bone microenvironment fluctuate, increasing the first day after the trauma occurs, and again between 14 and 21 days post trauma.[39] Similarly, VEGF concentrations during wound healing varies, reaching a peak between 3 and 7 days after injury, after which concentrations decrease.[37] There are several other tissues that demonstrate hierarchical variations in ECM proteins that are key to their overall function. The blood vessel's tunica intima for instance contains high elastin and collagen IV levels that provide the internal layer of the vessel with elasticity, the tunica media contains smooth muscle cells that inhabit an ECM composed of elastin sheets, collagen fibers and GAGs and the fibroblast-laden tunica adventitia owes its stiffness to its high collagen content.[25,26] The cardiac wall is composed of a range of ECM proteins, including a variety of collagens, aggrecan, fibronectin, and fibrillin. The orientation of these fibrillar proteins vary between the different regions of the cardiac wall (i.e., the epicardium, myocardium and endocardium), which is crucial for the overall mechanical function of the cardiac muscle.[40,41] In another example, the pericentral region of the liver (i.e., the area close to the central hepatic lobule vein) is rich in fibronectin and collagen I for mechanical strength, whilst the periportal region (i.e., the area surrounding the hepatic lobule vessels) is rich in laminin, collagen III, collagen IV and GAGs that provide elasticity to these regions.[42]

Table 1. Examples of tissue types wherein key variations exist within biochemical and biophysical cues that affect the local microenvironment of tissue zones and the overall tissue function. Biochemical cues are highlighted in yellow and biophysical cues are highlighted in orange. Glycosaminoglycan; GAG.

	Bone	
	Cortical bone	Cancellous bone
Biochemical cues		
ECM	Collagen I (85–90%), hydroxyapatite	Collagen I (85–90%), hydroxyapatite
Oxygen[19,20]	1–7%	2–7%
Biophysical cues		
Porosity[21]	5–15%	40–95%
Compressive mechanical properties[22]	130–200 MPa	0.1–16 MPa

	Cartilage				
	Superficial zone	Transitional zone	Deep zone	Calcified cartilage	Subchondral bone
Biochemical cues					
ECM	Collagen II (85%), GAG (15%)	Collagen II (67%), GAG (25%)	Collagen II, GAG (20%)	Collagen II/X, hydroxyapatite (65%)	Collagen I, hydroxyapatite (85%)
Oxygen[20]	6%	2%	1–2%	5%	5–10%
Biophysical cues					
Permeability[20,23]	$9.3*10^{-16}$ m^4 N^{-1} s^{-1}	$8.0*10^{-16}$ m^4 N^{-1} s^{-1}	$7.1*10^{-16}$ m^4 N^{-1} s^{-1}	$2.0*10^{-15}$ m^4 $N^{-1}s^{-1}$	$2.0*10^{-15}$ m^4 N^{-1} s^{-1}
Tensile mechanical properties[20]	42 MPa	13 MPa	2.6 MPa	50–100 MPa	50–100 MPa

	Blood vessels		
	Tunica intima	Tunica media	Tunica adventitia
Biochemical cues			
Cells	Endothelial cells	Smooth muscle cells	(Myo)fibroblasts
ECM[24,25]	Elastin, fibronectin, fibrillin, fibulin, collagen I-VI, GAG		
Biophysical cues			
Compressive mechanical properties[26]	0.16 MPa	0.84 MPa	0.90 MPa

Macromolecular Bioscience
www.mbs-journal.de

In addition to biological macromolecules, inorganic components present in the microenvironment assist in regulating tissue homeostasis. Phosphates play a crucial role in regulating calcification and bone resorption, inhibiting the recruitment and differentiation of osteoclasts and promoting cellular apoptosis.[43,44] Oxygen also plays a key role in regulating tissue homeostasis. Within the human body, the oxygen tension is typically between 1% and 14% partial oxygen pressure, however this varies both between tissues type and within regions of tissues.[45] For instance, articular cartilage is generally considered a physiologically hypoxic tissue, which presents a gradient of oxygen tension ranging from <10% at its surface to <1% in the deepest layers.[21] In comparison, bone is a highly vascularized tissue, where oxygen tension varies from 5% to 10%.[21] Hypoxia is a potent driver of cellular functions, influencing progenitor cell differentiation and the maintenance of the acquired phenotype, as well as ECM production in cartilage and other tissues.[46] Additionally, variation in levels of hypoxia levels within the tissue microenvironment can induce neo-angiogenesis and vasculature remodeling.[47,48]

2.2. Biophysical Cues

Biophysical cues, such as mechanical load and ECM stiffness, are recognized as key regulators of the tissue microenvironment. Changes in the mechanical load tissues experience can have a significant impact on musculoskeletal tissue architecture, both at the macroscopic level and microscopic level. Reduced loading induces rapid bone loss and cartilage atrophy, whereas high-impact loading can lead to stress fractures and cartilage degradation.[49–52] Cells can locally sense mechanical stress levels through mechanosensors that are present on the cell membrane. The activation of these sensors directly influences cell differentiation and ECM protein synthesis.[53–56] In addition to mechanical loading, resident cells are also highly responsive to variations in local ECM stiffness.[57,58] Each tissue is characterized by a specific ECM stiffness, which varies from soft (e.g., brain and liver, 0.1–10 kPa), moderate (e.g., muscles, 50–500 kPa) or stiff (e.g., bone 900–20*10^6 kPa).[53] Cell–substrate interactions are mediated by integrin receptors, triggering the formation of focal adhesions across the cell surface and the reorganization of their cytoskeleton.[53,59] Cell adhesion to softer or stiffer substrates can induce the formation of stable or dynamic focal adhesions, which in turn influences cell migration, differentiation, spreading and proliferation.[60] Durotaxis, stiffness-sensitive cellular movement, is highly cell-dependent and the absolute stiffness values that trigger cell migration may vary between cell types.[61] It has been shown that when exposed to stiffness gradients, fibroblasts and mesenchymal stromal cells (MSCs) prefer to migrate toward regions of increased stiffness (stiffness gradient ranging up to 12–34 kPa).[53,62,63] Furthermore, there is a large body of evidence to suggest that ECM stiffness influences cell differentiation toward several lineages, including neuro- (<1 kPa), adipo- (≈3 kPa), myo- (≈12 kPa), chondro- (<20 kPa), and osteogenic (<30 kPa) cells.[53,57,64–67]

In addition to local changes in mechanical loading and stiffness, other biophysical cues influence cell responses within the microenvironment. ECM viscoelasticity, a time-dependent response to loading or deformation, plays a crucial role in driving broad changes in gene expression, proliferation, migration and differentiation, independently from matrix stiffness.[4,68] Furthermore, changes in local viscoelastic behavior has been associated with the progression of pathological conditions, such as tissues fibrosis,[68] atherosclerosis,[69] osteoporosis,[70] and cancer metastasis.[71] The spatial organization of molecules within the ECM also regulates tissue development and homeostasis. Alignment of ECM nanofibrils directs the migration of different cell types (including fibroblasts, endothelial cells, and MSCs) through a process known as contact guidance.[72–75] Specifically, contact guidance triggers a reorganization of the cell cytoskeleton, which promotes alignment and migration along the topographical cue and inhibits orthogonal movements.[75–77] Finally, microenvironment permeability, defined as the accessibility to different molecules (e.g., nutrients and oxygen), regulates hypoxia-related cellular responses and cell metabolism.[78]

2.3. Physico-Chemical Gradients across Native Tissues

To allow complex biological functions to take place, different tissues interact and communicate through distinct tissue interfaces. Transitional areas such as the cartilage-to-bone transition in the osteochondral unit, or the tendon/ligament-to-bone interface at the muscle insertion site[5] are highly heterogeneous microenvironments, presenting gradients of biophysical and biochemical cues.[21] The osteochondral interface gradually transitions from stiff, highly vascularized bone tissue to viscoelastic, avascular cartilage tissue.[21] The various zones of tissues such as cartilage and blood vessels are also defined by the varying alignment and composition of the ECM that results in zonal variations in oxygen levels, porosity, and stiffness.[21,79] Similarly, the liver lobule naturally contains an oxygen gradient between the liver lobule's central vein and peripheral vessels that is thought to play a key role in its physiological function.[80] Injury sites such as a border zone after myocardial infarction also present biophysical gradient.[81]

Overall, the large range and spatial-organization of physico-chemical cues across a wide range of tissues play a key role in the functionality of these tissues.[82] It is therefore essential to develop and exploit tools that allow us to mimic these complex microenvironments, including spatial control over the various cues (i.e., biological, biophysical and ECM-based).

3. The Toolbox to Tailor Microenvironment Cues in Hydrogels

Recent developments in macromolecular chemistry has enabled the design of hydrogel microenvironments that possess a range of biophysical and biochemical cues, mimicking properties of native tissue niches.[3] To understand how spatiotemporal control over these cues can be achieved within cell-laden hydrogels, the relative contribution of each component and fabrication process of hydrogel precursors should be considered. The tools at our disposal that define hydrogels properties include the 1) choice of polymer, 2) grafting of functional end-groups on polymers to enable the use of specific crosslinking chemistries, 3) initiation mechanism of crosslinking, and 4) chemical incorporation

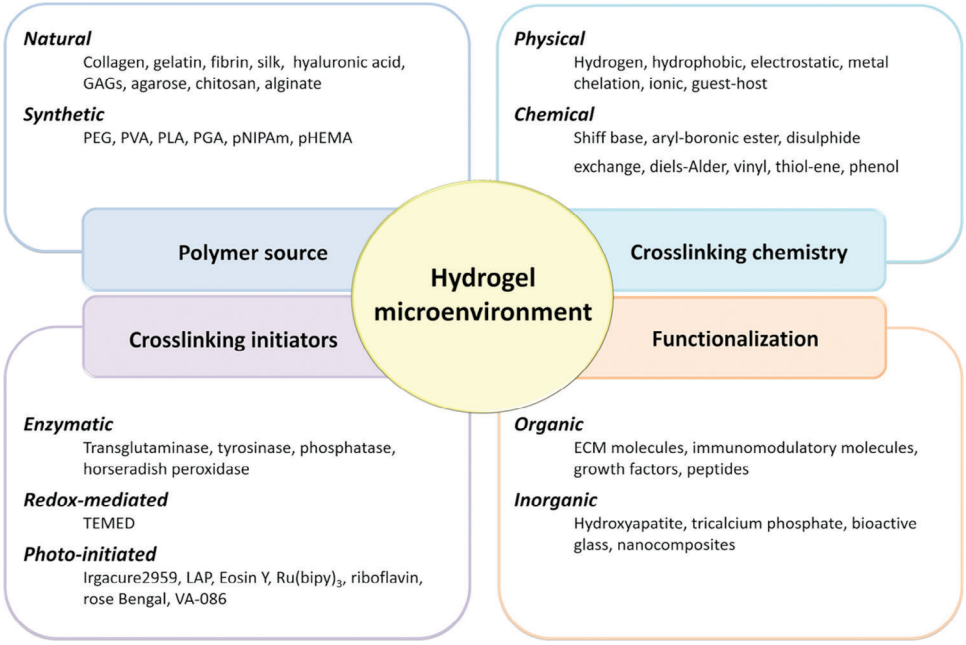

Figure 1. Schematic of parameters that influence hydrogel microenvironments, which can be tailored to achieve biomimicry. By selecting different polymer sources, crosslinking chemistry, initiators and functionalization, it is possible to reproduce specific physico-chemical properties of native tissues. 2,2′-Azobis[2-methyl-*N*-(2-hydroxyethyl)propionamide]; VA-086, glycosaminoglycan; GAG, 2-hydroxy-4′-(2-hydroxyethoxy)-2-methylpropiophenone; Irgacure2959, lithium phenyl-2 4 6-trimethylbenzoylphosphinate; LAP, *N*,*N*,*N*′,*N*′-Tetramethylethylenediamine; TEMED, Tris(bipyridine)ruthenium(II); $Ru(bipy)_3$.

of bioactive molecules (**Figure 1**). In this section, the relevance of each factor on the biophysical and biochemical properties of the hydrogel microenvironment is discussed using key examples.

3.1. Polymer Source

Hydrogels can be fabricated using polymers from biological or synthetic origin, each possessing different characteristics which can be exploited to trigger specific biological effects.[3] Biological polymers, such as collagen, gelatin, silk fibroin, chitosan, alginate, and hyaluronic acid (HA) are attractive options, as these molecules are already part of the native ECM microenvironment.[83] They are inherently cytocompatible and bioactive as they contain cell-adhesive moieties and enzyme-degradable bioactive sequences which will become part of the hydrogel backbone, and they exhibit viscoelastic properties which resembles those of native tissues.[83] However, biological polymers present several limitations, including low mechanical stiffness and batch-to-batch variability which translates to poor experimental reproducibility.[3,84] While addition of engrafted functional groups can alleviate the low mechanical stiffness of these polymers, this process is limited by the availability of pendent reactive sites on the polymer backbone.[85]

Synthetic polymers, such as poly(ethylene glycol) (PEG), poly(vinyl alcohol) (PVA), poly(lactic acid) (PLA), and poly(glycolic acid) (PGA), provide more controlled and reproducible biophysical and chemical properties (i.e., chain size, structural composition and availability of functional groups).[3] Nevertheless, they are often bioinert as they lack sites for cell adhesion and migration, potentially hindering their integration with the host tissues.[86] For this reason, synthetic polymers are further modified to incorporate network characteristics which are typical of biological polymers, like enzyme-specific degradation sequences and cell adhesive motives.[87–89]

Biological and synthetic polymers can be combined to form multipolymer networks, also known as hybrid networks. Hybrid networks combine the advantages of both polymer types, while mitigating their disadvantages.[83] For instance, incorporation of a small percentages of gelatin within a PVA polymer network significantly improves cellular interaction, without compromising the tailorable degradation profile and biophysical characteristic of the hydrogels.[87] PVA hydrogels containing chondroitin sulfate (CS) and collagen II had demonstrate enhanced integration in osteochondral defects and influences hydrogel degradation rates.[90]

3.2. Crosslinking Chemistry

Polymer crosslinking is essential to achieve hydrogel formation, converting the soluble polymers into a more stable network, with high water content. Crosslinking density represents the number of crosslinks per unit volume in a polymer network and is a major factor influencing hydrogel properties across all crosslinking methods. The crosslinking density influences the hydrogels porosity, pore size, and effective hydrogel stiffness (as higher crosslinking densities restrict polymer network swelling, providing the hydrogel with higher overall stiffness).[3,91] These properties are known to significantly impact cellular behavior,

influencing migration, metabolism and differentiation.[92,93] The method utilized for hydrogel fabrication defines the nature of these crosslinks, and together with the crosslinking density defines biophysical properties of the hydrogel and therefore the engineered microenvironment. Crosslinking methods can be grouped into two main categories, biophysical and chemical/covalent crosslinking, described below.

3.2.1. Physical Crosslinking

Physical crosslinks within hydrogels are reversible and are induced by environmental factors, such as temperature, pH, and ions.[94] Variations in these factors trigger the formation of non-covalent interactions, such as ionic interactions, hydrogen bonding, hydrophobic association, and van der Waals attractions or chain entanglement. The resulting supramolecular hydrogels are dynamic in nature, as the bonds that constitute the polymer network are reversible and are characterized by an equilibrium association constant (K_{eq}) and binding kinetics related to the rate constants of association and dissociation.[94] These constants influence hydrogel attributes, including stress relaxation (i.e., breakage of dynamic bonds under stress) and self-healing (i.e., recovery of dynamic bonds after stress recovery).[95] The K_{eq} defines the overall hydrogel physico-chemical and mechanical properties, including hydrogel porosity and stiffness. Stable hydrogels formed through reversible physical interactions are known as supramolecular hydrogels and the considerable flexibility and versatility they offer are particularly appealing for TE applications.[94] The self-assembly and gelation processes of supramolecular hydrogels is often reliant on the simultaneous action of multiple synergistic non-covalent interactions, with key examples below.

Peptide amphiphiles are small peptides that consist of an amino acid sequence that is bound to a terminal fatty acid, and exploit **hydrophobic interactions**.[96] In aqueous solution peptide amphiphiles self-assemble, orientating their hydrophilic amino acids toward the solvent while the fatty acids face inward, forming a fatty acid core.[96] An interface is formed between the solvent and the peptide amphiphiles s which results in the formation of a hydrogel network made of nanofibrils with sizes that can be tailored through adjusting the peptide amphiphiles sequence and size, but generally falling within 5–8 nm in diameter. Due to nanofibril formation, peptide amphiphiles-based hydrogels have the potential to mimic the fibrillar nature of the native ECM.[97] Bulk hydrogel properties can be adjusted by altering the bulk solution ionic strength and concentration, or by adjusting the peptide amphiphiles hydrophilic amino acid length.[98,99]

Elastin-like proteins (ELPs) are characterized by repeating VPGXG sequences (wherein X is an undefined amino acid residue) and rely on **hydrogen bonding** to form a crosslinked hydrogel network.[100] As hydrogen bonds are weak, ELP-based hydrogels are generally soft (<1 kPa) and are mainly applied for soft tissue engineering (i.e., neural engineering), but their use has been explored for cartilage engineering.[100,101] Due to the inherent low stiffness of ELP-based hydrogels, they often demonstrate limited structural fidelity, which can be overcome by combining ELPs with other polymers. ELPs have been modified with hydrazines and used as crosslinkers for aldehyde-modified HA, resulting in stable hydrogel formation through a Schiff base reaction which supported fibrocartilage formation.[102]

Chitosan and alginate are biomaterials which use **electrostatic and ionic interactions** to fabricate hydrogels. The electrostatic interactions of chitosan, a polycationic polysaccharide, arise from its amino groups and forms low mechanical stability hydrogels.[103] For this reason, electrostatic interactions are often exploited to form a network between chitosan and anionic groups present on secondary synthetic polymers (such as PVA and PEG) or biological polymers (such as collagen).[103–105] Alginate hydrogels are formed through ionic interactions between guluronic acid blocks on the alginate backbone and cations such as calcium, barium, and zinc.[106] Alginate and chitosan are particularly attractive biomaterials when aiming at tailoring the cellular microenvironment of hydrogels for engineering purposes, as their physical properties can be tailored by simply by varying the extent of electrostatic and ionic interactions.[106] The biological and physical properties of chitosan hydrogels can also be adjusted by altering the isolation protocol of the polymer from the shells of sea creatures through the deacetylation of chitin. By adjusting the extent of deacetylation, hydrogel properties such as cell adhesiveness, degradation profile and stiffness can be customized for specific applications.[107,108] Similarly, stiffness and viscoelasticity of alginate hydrogels can be tailored through adjusting the molecular weight of the polymer and the type or concentration of the cations taking part in the gelation process.[109,110]

Supramolecular hydrogels can also be fabricated exploiting **guest–host interactions**, which entails the presence of structurally well-defined guest molecules, which is included within the "cavity" of the host molecule. The host molecule typically contains a recognizable supramolecular motif and the interactions between the two components are often of a hydrophobic nature.[111,112] Guest and host molecules can be natural (i.e., cyclodextrin) or synthetic (i.e., ureidopyrimidinone, cucubtrils, and benzene-tricarboxamides) and are commonly grafted to backbones of polymers such as PEG, alginate and HA to fabricate hydrogel networks.[113] The stiffness and viscoelasticity of the resulting hydrogel is dependent on the affinity between guest and host as evidenced by a study in which the physico-chemical properties of hydrogels containing a cucubtril-based host molecule and a range of guest molecules were probed. The guest–host pairs with a high binding affinity (higher K_{eq}) lead to the fabrication of hydrogels with higher stiffness and reduced viscoelasticity.[114] High binding affinity results in slower stress relaxation and self-healing, as a result of the reduced dissociation rates of the guest-host complex.[114] The stiffness of supramolecular hydrogels fabricated exploiting guest–host interactions can be further tailored by using multivalent guest crosslinkers that interact with multiple host molecules grafted on the polymer backbone. Cyclodextrin has been used as host molecule on an alginate backbone, with adamantane as a guest molecule. Bi- or multifunctional PEG molecules for instance were functionalized with adamantane to generate multivalent guest crosslinkers, which resulted in an increase in both K_{eq} and hydrogel stiffness as a function of increasing crosslinker functionality.[115]

3.2.2. Chemical Crosslinking

Covalent bonds are characterized by their irreversibility and excellent bond strength (220-570 kJ mol^{-1} bond energy). Hydrogels formed though rigid covalent bonds generally possess higher mechanical properties and stability compared with hydrogels based on physical interactions.[116,117] They therefore achieve more stable hydrogel shapes and provide structural support to the encapsulated cells during long-term cell culture. Several strategies can be exploited to fabricate hydrogels via covalent crosslinking, including homo-polymerization of vinyl groups (i.e., acrylates or methacrylates) and the interactions between thiols and alkenes, through thiol-ene click chemistry.[10,118–120]

The homo-polymerization of vinyl groups occurs through a process known as chain-growth polymerization, where free radical species are typically utilized for the initiation of the crosslinking (i.e., free-radical **chain-growth polymerization**). Free radicals react with vinyl groups on the polymer backbone to form a carbon-centered kinetic chain that propagates along further vinyl residues.[118] As the reaction proceeds and more reactive intermediate centers are formed, random radical chain termination can occur when two chain ends meet. As chain-growth polymerization is a thermodynamically driven process where random chain termination can occur, hydrogels formed through this mechanism are generally heterogeneous in their crosslinking density.[120] Different initiation mechanisms exist for chain-growth polymerization that involve the photolysis of an anionic initiator into a Lewis base, or cationic initiator into a Lewis acid, to initiate crosslinking.[121] These processes, termed anionic and cationic chain-growth polymerization respectively, are nevertheless less compatible with cells, as they generally require strong acids/bases and/or polar solvents for hydrogel formation.[122]

Thiol-ene click chemistry proceeds through a different crosslinking mechanism, known as **step-growth polymerization**. In this reaction, alternating propagation and radical chain transfer steps result in the formation of thioether bonds.[123] Consequently, termination does not occur during step-growth polymerization, thereby making this process not susceptible to the same random variations in crosslinking described for chain-growth polymerization. The uniformity of crosslinking is dependent on the structure of the polymer, functional groups and crosslinker, as well as the location and availability of functional groups.[124] The impact of polymer network homogeneity on cell behavior has been recently investigated by comparing cellular morphology in chain-growth polymerized PEG-methacrylate (PEG-MA) and step-growth polymerized norbornene-terminated PEG (PEG-NOR) hydrogels with similar bulk mechanical properties.[124] The crosslinking method results in significant variations in the microscale hydrogels physico-chemical properties, with high local stiffness variations and the formation of local hydrophobic pockets in chain-growth polymerized hydrogels—leading to reduced cell attachment and spreading.[124] Nevertheless, contrasting evidence suggests that network heterogeneity can be beneficial for tissue formation, as local variations in the microenvironment can induce cellular traction and phenotypical changes. While it is thus clear that the crosslinking mechanism crucially affects the resulting microenvironment that encapsulated cells observe, debate remains as to which mechanisms are best suited toward replicating specific tissue types.

3.2.3. Dynamic Covalent Bonds

Dynamic covalent bonds are an intermediate form of bond, which present properties that are typical of both physical and covalent bonds. Specifically, dynamic covalent bonds are generally less strong than rigid covalent bonds but higher bond energies can be achieved compared to those observed for physical bonds.[125] Similar to the supramolecular bonds, dynamic covalent bonds demonstrate non-constant bond kinetics, characterized by a K_{eq} and association/dissociation constants. Hydrogels crosslinked using dynamic covalent bonds therefore have stress relaxation and self-healing properties, which are dependent on the bond kinetics.[125,126] However, the selection of the dynamic bond greatly influences hydrogel properties such as hydrogel stiffness, viscoelasticity, self-healing, cell morphology, and printability.[126] By exploiting different imine-type dynamic covalent chemistries to crosslink aldehyde-modified alginate hydrogels, oxime, semi-carbazone, and hydrazine bonds can be achieved. Hydrogel stiffness and K_{eq} varied by bond type—oximes > semi-carbazone > hydrazone,[126,127] and differences in viscoelasticity and in stress relaxation were observed, with the oxime-crosslinks most stable and showing reduced stress relaxation.[127] Similarly, the association rate (through condensation) is reduced in oxime bonds, reducing the rate of self-healing, or preventing self-healing from occurring at all.[126] Interestingly, these difference in physical properties led to changes in cell morphology, with fibroblasts spreading in hydrazine-crosslinked hydrogels, but not in oxime-crosslinked hydrogels.[126]

3.3. Crosslinking Initiators

Crosslinking can be initiated through three main mechanisms, 1) enzymatically, 2) through the use of redox reactions, or 3) through photoinitiation. The selection of different initiators influences hydrogel stiffness, swelling and long-term stability.[128–130] These properties can be spatially controlled to different various degrees, favoring the fabrication of hydrogels with homogeneous or heterogeneous properties. Importantly, understanding the impact of initiators and by-products of the crosslinking reaction on cell viability and behaviors is an important consideration in the design of cell-laden hydrogels.

3.3.1. Enzymatic Crosslinking

Enzymatic crosslinking of hydrogels is popular due to relatively fast gelation times, excellent biocompatibility and the possibility of triggering in situ polymerization.[131] Enzyme-mediated crosslinking usually triggers the formation of covalent bonds between residues, which are commonly found on specific biological polymer backbones.[131] Transglutaminases facilitate covalent bond formation between glutamines (carboxamides) and lysines (primary amines), whereas tyrosinases, lysyl oxidases and horseradish peroxidases induce the crosslinking between tyrosine/lysines and lysines and hydroxyphenyls, respectively.[17,132,133] Fibrin, for instance, has been studied widely within tissue engineering as a biopolymer that can be crosslinked enzymatically through the formation of fibrin polymers from

cleavage of fibrinogen by the enzyme thrombin[134] and can subsequent be crosslinked by transglutaminase to form a fibrin hydrogel.[135] The main disadvantage of enzymatic crosslinking of natural polymers is the variable physical properties of the resulting hydrogel, as the extent of crosslinking is dependent on the abundance of specific amino acids on the polymer backbone, which may vary between sources and batches of polymers. To achieve enhanced control and reproducibility over the hydrogel physico-chemical properties, natural and synthetic polymers have been functionalized with known amounts of specific moieties for enzymatic crosslinking. Tyramine-functionalized collagen I aided in tailoring the mechanical properties and hydrogel degradation rates, and promoted chondrocyte differentiation and matrix deposition for cartilage engineering.[132] Similarly, PEG and chondroitin sulfate can be functionalized with transglutaminase factor XIII specific substrate sequences to allow controlled crosslinking between macromolecules, forming a hydrogel with defined properties and localized release of biological cues for bone engineering applications.[133]

3.3.2. Redox/Photo-Mediated Crosslinking

Redox- and photo-initiators are able to initiate crosslinking through the generation of free radicals.[6,136] Common systems that exploit redox crosslinking use *N,N,N′N′*-tetra- methylenediamine, which accelerates the decomposition of peroxydisulfates such as ammonium persulfate and leads to the formation of sulfate radicals that can initiate chain- and step-growth polymerization.[137] Photo-initiators provide rapid formation of free radicals in response to photon-induced excitation of photo-initiators. While redox- and light-based initiators are more widely applicable compared to enzymatic initiators, radical-induced cytotoxicity can occur if the free radical generation and radical consumption are not carefully matched.[6,138,139]

In recent years, photo-polymerization has attracted much attention within the engineering sphere for the formation of hydrogels, owing to the enhanced spatiotemporal control provided compared to redox- and enzymatic initiators.[136] For that reason, photo-based initiation is the most attractive option when looking to design a covalently crosslinked microenvironment that mimics the spatial variations present in native tissue. Photo-initiators need to satisfy several criteria, such as solubility in aqueous solvent, cytocompatibility and the ability to absorb photons and produce initiating radicals.[6,139] Several photo-initiators have been adopted for the formation of cell-laden hydrogels, including 2-hydroxy-4′-(2-hydroxyethoxy)-2-methylpropiophenone (Irgacure 2959),[140] lithium phenyl-2,4,6-trimethylbenzoylphosphinate,[141] camphorquinone,[142] Eosin Y[143] and co-initiator triethanolamine,[5] and Tris(2′-2′-bipyridine)ruthenium(II) and co-initiator sodium persulfate.[144] The absorbance wavelength of the photo-initiator is a key consideration and typically lies within the ultraviolet (UV) (200–400 nm) or visible (400–800 nm) light spectra.[6] An upper limit in applicable wavelengths exist due to light absorption by water (>900 nm).[145] Visible light is generally preferred given that UV exposure can cause chromosomal and genetic instability in cells and may consequently result in cytotoxicity.[6,138,146] It has also been suggested that heat-induced cytotoxicity can occur due to light irradiation, but to date the interplay between irradiation wavelength and heat generation and the downstream implications on cell viability and cell behavior has not been fully characterized.[147] One of the most important considerations when selecting photo-initiators is their final intended application. If aiming at engineering large constructs or at transdermal photo-polymerization (i.e., photo-polymerization of a hydrogel precursor solution after injection under a skin layer), light penetration depth should be considered. Higher wavelength light travels further through tissues and larger engineered constructs,[148,149] demonstrating that visible light-sensitive photo-initiators are preferred over UV-light sensitive ones to ensure complete crosslinking and the formation of hydrogels with homogeneous physical properties.[148–151]

3.4. Functionalization with Bioactive Molecules

Incorporating bioactive cues within the hydrogel microenvironment can promote several biological effects.[152] Depending on the final application, various cues can be integrated into the polymer networks, including ECM proteins, peptide sequences that mediate cell adhesion or activate enzyme-mediate degradation, growth factors, and immunomodulatory molecules and inorganic components (i.e., hydroxyapatite).[152–156] The simplest method to incorporate bioactive cues is through direct loading, whereby macromolecules of interest are physically entrapped in the polymer network and the duration of their biological effect is dependent on their passive diffusion out the hydrogel.[157] This can be tailored to a certain extent by changing the crosslinking density and the pore size of the network or by exploiting intermolecular interactions like electrostatic and hydrophobic interactions between the polymer and the bioactive cue.[157,158] Covalent incorporation strategies are used to achieve additional spatial and temporal control over the cell exposure to biological cues, through the use of spacer molecules or direct binding to the polymer backbone.[159,160] A common example of this conjugation modality is the use of methacrylated gelatin and acrylated or methacrylated primary amines of growth factors, which undergo free radical polymerization in the presence of a photo-initiator and UV irradiation.[159,161] PEG hydrogels can be produced by photoinitiated step-growth polymerization by reacting PEG-NOR with a dithiol PEG crosslinker. Thiolated transforming growth factor β1 (TGF-β1) can then be conjugated to PEG-NOR by thiol-ene click reaction.[162] Nevertheless, chemical modification of biological macromolecules can affect their functionality, either through cross-reactive reagents using during the process or due to alteration of protein 3D structure.[163–165] To overcome this challenge, methods to functionalize synthetic or natural polymers networks with pristine ECM molecules or growth factors have been developed. Ruthenium and sodium persulfate-mediated visible light crosslinking has been used to enable the formation of bi-phenol crosslinks between tyraminated PVA and growth factor tyrosine groups in a rapid and controllable manner.[130] Nevertheless, all immobilization strategies inhibit macromolecules internalization which promotes the sustained activation of intracellular signaling pathways. However not all growth factors act in the same manner and in some cases growth factors internalization is required in order to properly exert their

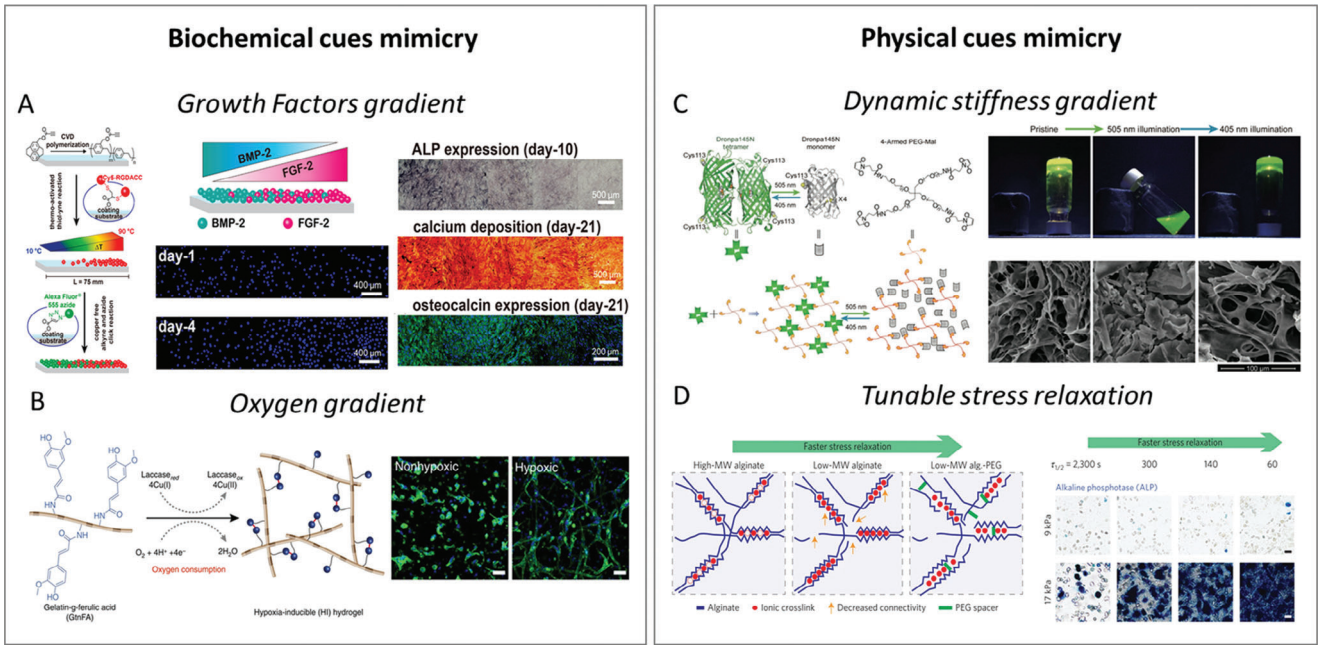

Figure 2. Examples of biochemical and biophysical cues which are mimicked and controlled in specific gradients within tissue engineered constructs through manipulating macromolecular chemistry. Biochemical cues include A) growth factor gradients. Adapted with permission.[169] Copyright 2016, American Chemical Society. B) Oxygen gradients. Adapted with permission.[170] Copyright 2014, Springer Nature Limited, while biophysical cues include C) dynamic stiffness gradients. Adapted with permission.[171] Copyright 2018, Tsinghua University Press and Springer-Verlag GmbH Germany, part of Springer Nature. D) Tunable stress relaxation. Adapted with permission.[109] Copyright 2015, Springer Nature Limited. Bone morphogenic protein type 2; BMP-2, fibroblast growth factor type 2; FGF-2, poly(ethylene glycol)-maleimide; PEG-Mal.

effects.[152] An alternative strategy to ensure prolonged and controlled release of bioactive molecule is to exploit affinity sequestration, where ECM molecules, or mimetics, are incorporated in the polymer network and act as a reservoir of growth factors. Heparin, fibronectin and collagen are among the most studied ECM molecules for this application, as they have shown the ability of binding a wide range of growth factors and immunomodulatory molecules, including BMP-2, TGF-β1 and platelet-derived growth factor (PDGF), making them particularly versatile for musculoskeletal tissue engineering applications.[152,166–168]

4. Macromolecular Chemistry to Achieve Microenvironment Biomimicry

Biomimetic hydrogels can be fabricated as tools in fundamental studies which explore the effects of specific stimuli on native tissue physiology and tissue healing, and provide critical information for the rational design of ad hoc regenerative strategies. This section provides specific examples of where precise combinations of polymers, crosslinking strategies, crosslinking initiators and network functionalization result in the successful recapitulation of specific physical and/or biochemical properties of native tissues microenvironments, with either homogeneous properties or heterogeneous interfaces (**Figure 2**).

4.1. Biomimicry of Biochemical Cues

Biochemical cues, such as growth factors, are commonly present in the native microenvironments to guide cell behavior and are often compartmentalized, especially at tissue interfaces.[3,5] Crosslinking chemistries can be combined to recapitulate the heterogeneous distribution of biochemical factors, recreating physiological gradients.[3,169,172]

During tissue healing, MSCs are commonly recruited to the injury site and to promote this step in tissue-engineered constructs several studies have focused on the design of specific gradients to attract MSCs. Atallah et al. developed a PEG-GAG hydrogel with tuneable GAG sulfation patterns, which was exploited to sequester PDGF. Gradual release of PDGF into a neighboring MSC-laden hydrogel resulted in a PDGF gradient that induced changes in MSC morphology and demonstrated a chemotactic effect.[172] More complex gradients have been designed to trigger multiple biological effects at the same time. To promote both cell recruitment and mimic spatially organized gradients of osteogenic growth factors for bone regeneration, Guan et al. employed click chemistry reactions triggered by different conditions (i.e., thiol-ene or copper-free alkyne and azide reaction) to engineer two reverse gradients of fibroblast growth factor 2 and BMP-2 (Figure 2A).[169] These two counter-current distributions of growth factors induced adipose-derived stem cell (ASC) proliferation on half of the construct and osteocalcin expression and tissue mineralization on the other.[169] However, both the spatial confinement of growth factors and their controlled temporal release is crucial for triggering the desired biological effect. Lienemann et al. evaluated the effect of simultaneous or sequential release of PDGF-BB and BMP-2 on bone formation and found that when both growth factors were released at the same time, PDGF inhibited BMP-2-mediated osteogenesis both

in vitro and in vivo.[173] Utilizing a two-way dynamic release system with fast-release of PDGF and sustained delivery of BMP-2 (which was immobilized within the polymer network) enhanced healing in bone defects. The generation of biochemical gradients with temporal control have also been established through development of hypoxia-inducible hydrogels, which are formed with in situ oxygen consumption via a laccase-mediated reaction (Figure 2B).[170,174,175] Oxygen levels can be accurately predicted by mathematical models and exploited for fundamental studies or to promote vascular infiltration during wound healing for tissue engineering applications.[170,174]

4.2. Biomimicry of Biophysical Cues

As detailed in Section 2.2, key physical properties of tissue microenvironments include mechanical stiffness, ECM viscoelasticity, ECM alignment and matrix permeability. Diverse microenvironment stiffnesses can be achieved in several ways; for example, by combining multiple polymers to form an interpenetrating network or by increasing the polymer density, crosslinking conditions and initiator concentrations.[3,128,176,177] Hydrogel stiffness plays an important role in driving differentiation of MSCs and ASCs toward osteogenic or chondrogenic lineage, for bone and cartilage tissue engineering applications, respectively.[178–181] Furthermore, local tuning of microenvironment stiffness creates gradients which can be exploited to influence cell migration through durotaxis and promote cell recruitment within the engineered tissues (Figure 2C).[153,171] Early hydrogel models with engineered stiffness gradients were fabricated simplistically by mixing soft and stiff pre-hydrogel formulations, creating poorly characterized stiffness gradients. To achieve more defined and controlled stiffness gradients, light irradiation can be manipulated in photo-polymerizable hydrogels using a sliding mask to form variable crosslinking densities.[182] More recently, a double-layered polyacrylamide gradient hydrogel also showed tuneable gradient strengths with high reproducibility.[67] The rate of durotaxis increases in hydrogels with soft initial stiffness and in gradient hydrogels with steep stiffness steps.[62,183–185] To study the direction of cell migration, Ehrbar et al. investigated the rational design of hydrogels to identify the type of migration occurring on different substrates.[153] Stoichiometrically balanced ([lysine]/[glutamine] = 1) 8-arm PEG macromers, containing pending factor XIIIa substrate peptides, were enzymatically crosslinked with/without a metalloproteinase-sensitive linker. Non-proteolytic migration was predominant in matrices of low stiffness, while proteolytic migration was observed in matrices of higher stiffness.

The viscoelasticity of hydrogels can be tuned by varying polymer source or modifying crosslinking conditions, with natural polymers often more viscoelastic than synthetic polymers.[3] Chaudhuri et al. investigated the effect of viscoelasticity on osteogenic differentiation in MSCs by manipulating alginate hydrogel design to tailor the stress relaxation of the polymer network without affecting hydrogels overall stiffness (Figure 2D).[109] Polymers of different molecular weights with varied crosslinking densities were manufactured using calcium ions and covalent coupling short PEG spacers, demonstrating that rapid stress relaxation promoted osteogenesis.[109] It is therefore important to consider how different polymer networks respond to cell-mediated stress, which can proceed through storage of stress in purely elastic hydrogels, or dissipation of stress in viscoelastic hydrogels.[109,186]

Polymer alignment and matrix permeability can also be tuned by tailoring different parameters within the macromolecular chemistry toolbox presented in Section 3. Anisotropic fibers and pore alignment have been achieved in type I collagen hydrogels by combining controlled fibrillogenesis and freeze casting methods, introducing ice crystals to guarantee a macro-porous structure.[187] The achieved alignment influences myoblast and fibroblast orientation and migration.[187] and Paracrine signaling and the extent of cell-to-cell contact is also dependent on polymer alignment and porosity, which can affect differentiation.

4.3. Biomimicry of Complex Microenvironments

While specific biochemical and biophysical cues have been incorporated and temporally/spatially controlled within tissue engineering constructs, the native microenvironment constitutes multiple cues, which act synergistically to drive complex cell responses. Rational design of hydrogel properties can be employed to mimic this complexity in vitro and to study the hierarchical importance of these cues for regenerating precise tissue. Stiffness gradients have durotactic effects on vascular smooth muscles cells, however this process is substrate dependent with migration observed on fibronectin-coated polyacrylamide hydrogels, but not on laminin-coated hydrogels.[188] Additionally, the durotactic effects observed in fibroblasts can be overruled by topological cues, migrating along convex features preferentially.[189] Perpendicular biological gradients can be engineered within a singular hydrogel and used as a screening tool for identifying synergies between peptides. Vega et al. utilized thiol-norbornene light-mediated reactions to crosslink norbornene-functionalized HA (HA-NOR) macromers with di-thiol crosslinkers to understand the effects of cell–cell (histidine alanine valine; HAV peptide) and cell–matrix (arginine glycine aspartic acid; RGD peptide) signals on MSC chondrogenesis.[190] High HAV and low RGD levels increased the expression of chondrogenic markers (Sox9 and Aggrecan) and promoted the production of GAGs and collagen II.[190] Finally, orthogonal gradients of mechanical and biochemical cues (i.e., RGD peptide) can be created using a photocontrolled thiol-ene radical reaction and photomasks that adjust the dose of UV light in each crosslinking step to decipher cell–niche interactions (**Figure 3**).[191]

5. Beyond the Microenvironment: Macroscopic Tissue Organization

While at the microscale, tissue physiology and homeostasis are preserved by a plethora of cellular, biochemical and biophysical cues, macroscale organization of tissues is also essential to drive function.[5,13,19,82] Advancements in the field of biofabrication have meant that mimicking the macro-architecture of native tissues is more feasible, with different techniques offering varying degrees of spatial control over patterning of 3D cell-laden hydrogels (**Figure 4**A).[82,192,193] By rationally designing the

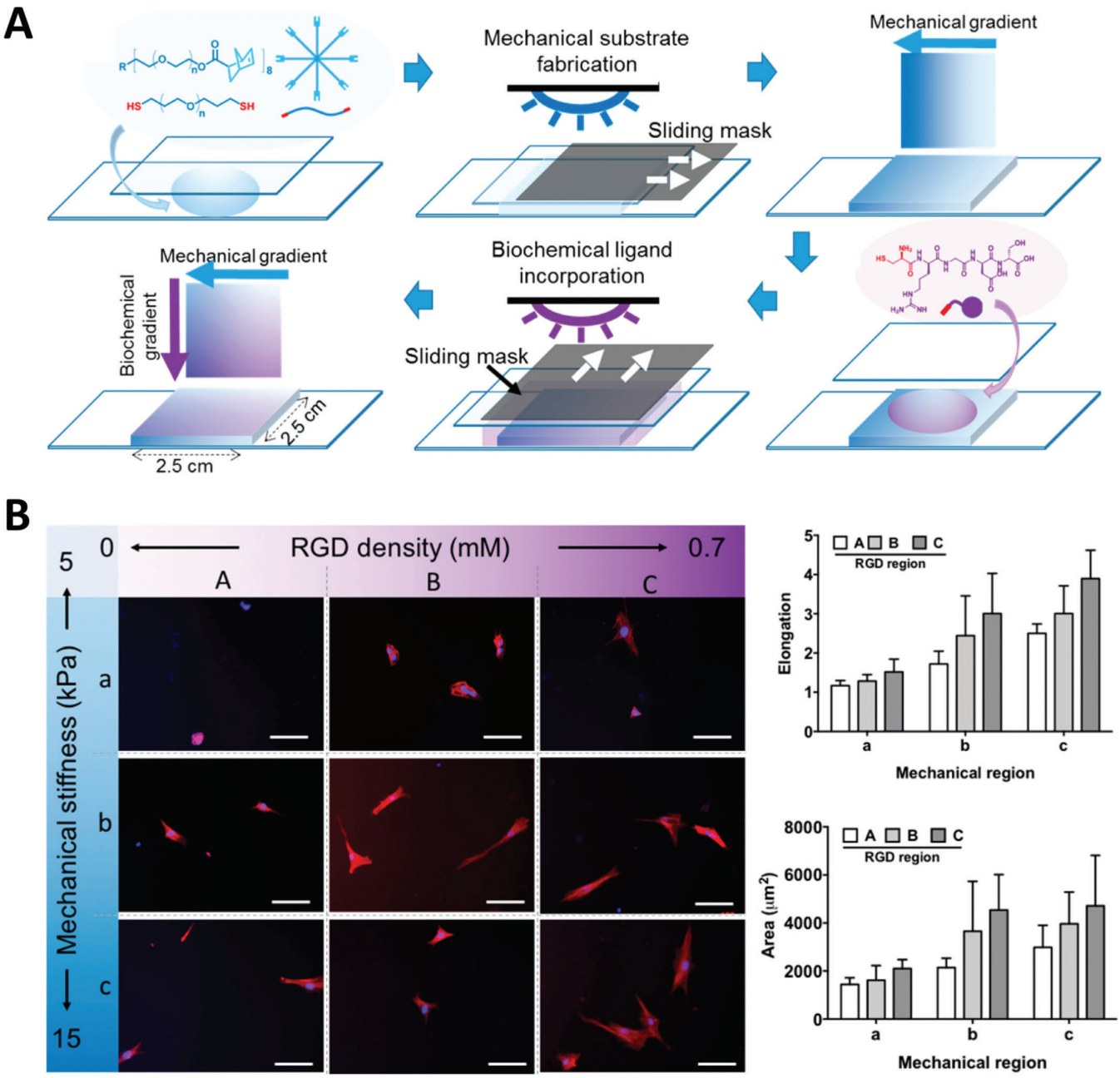

Figure 3. Complex microenvironments fabricated to mimic physiological conditions by incorporating both variations in mechanical stiffness and RGD sequence density. A) Overview of the fabrication procedure and B) difference in cellular morphology observed in the gradients. Reproduced with permission.[191] Copyright 2016, American Chemical Society.

macromolecular chemistry underlining the development of biomimetic hydrogel bioinks and compatible biofabrication technologies, it is now increasingly feasible to reproduce properties within the micro- and macro-environment of native tissues (Figure 4B). In this section, examples are presented wherein macromolecular chemistries of bioinks has been considered within biofabrication-driven approaches to achieve hierarchical tissue biomimicry.

5.1. Extrusion-Based 3D Printing for Biomimicry of Tissue Hierarchy

Extrusion-based printing is the most adopted biofabrication technology and involves the deposition of a bioinks in a layer-by-layer fashion to build up a 3D construct. The major appeal of extrusion-based bioprinting is the relative ease of combining multiple bioinks that represent different physico-chemical properties

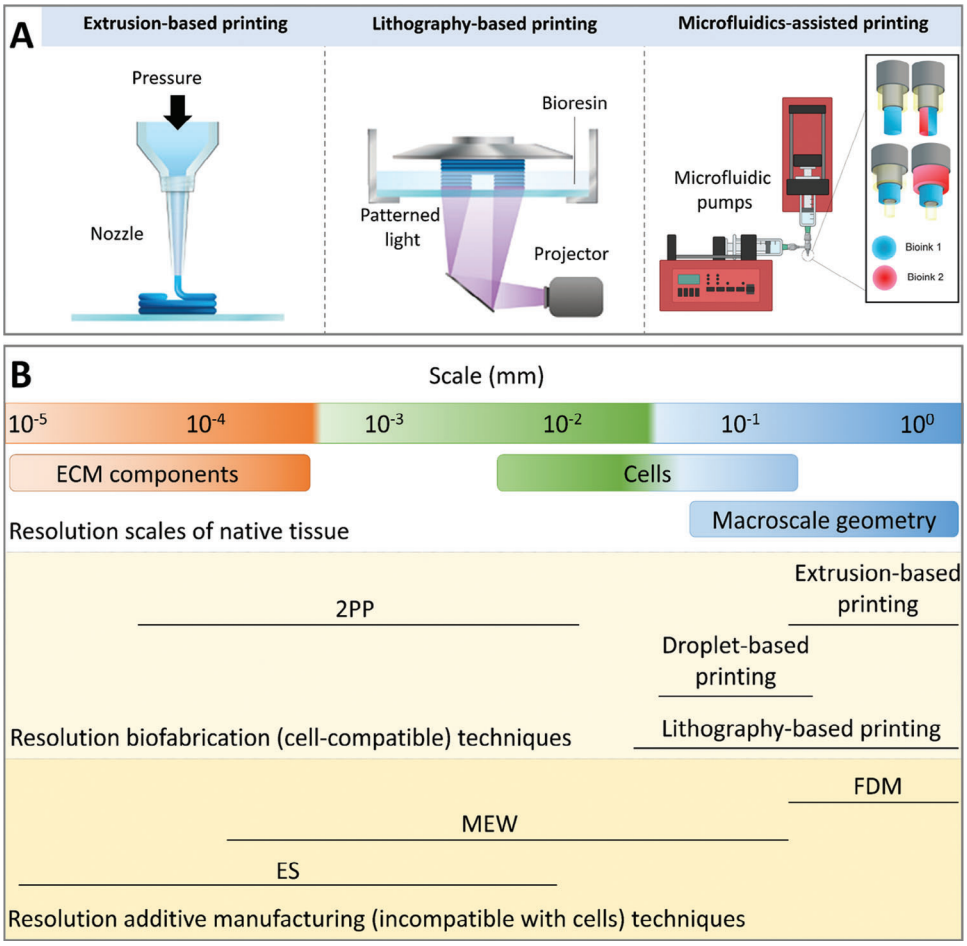

Figure 4. Schematic overview of biofabrication techniques and the scale that these techniques operate at. A) Commonly used biofabrication techniques include extrusion-based printing, lithography-based printing and microfluidics-assisted printing. Adapted with permission.[194] Copyright 2020, American Chemical Society. B) Overview of the resolution limits for different biofabrication techniques (i.e., techniques that allow for the incorporation of cells) and additive manufacturing approaches (i.e., techniques that provide spatial control but are incompatible with cells).[195] 2PP; two-photon polymerization, ES; electrospinning FDM; fused deposition modelling, MEW; melt electrowriting.

or encapsulating several cell types.[192,193] This approach allows replication of multiple properties from native microenvironments (i.e., tissue interfaces) in the same engineered construct. Motealleh et al. 3D-printed nanocomposite-laden alginate inks to achieve three separate zonal compartments with varying nanocomposite content.[196] The step-wise nanocomposite gradient guided fibroblast migration toward the construct layer with the highest nanocomposite content and promoted the migration and osteogenic differentiation of MSCs, where mineralized matrix deposition was evident in areas with high nanocomposite content.[196] Byambaa et al. created specific vasculogenic and osteogenic niches within the same construct by combining microscopic cues with precise macroscopic tissue organization to achieve functional vasculature within osteon-like structures composed of gelatin-methacryloyl (Gel-MA).[197] The Gel-MA concentration and the degree of functionalization were tuned within a pyramidal structure. The inner part of the construct was composed of a fast-degrading, soft (5%) Gel-MA with encapsulated human umbilical vein endothelial cells (HUVECs) and MSCs which formed vascular structures. The outer layers were composed of stiffer (10%) Gel-MA loaded with silicate nanoplatelets, to promote MSCs osteogenic differentiation, and with a gradient of covalently conjugated VEGF, to promote vascular infiltration.[197] Fabricating heterogeneous microenvironments within macroscopic constructs is important for promoting vascular networks within 3D-printed bone tissue analogues.[197–199] Similarly, hydrogel architecture (i.e., pore orientation) guides the self-assembly of microcapillaries which has been investigated by manipulating different design parameters within gelatin-norbornene (Gel-NOR)-based 3D-printed constructs.[10] While extrusion-based bioprinting technologies provides potential for combining micro- and macro-environmental cues, there are a range of design factors and challenges which need to be considered. Bioinks used for extrusion-based bioprinting need to conform to precise printability criteria, including adequate (high) viscosity (10^2–10^6 mPa s) to prevent sedimentation prior to extrusion, shear-thinning properties that allow the bioink to flow through the needle while limiting shear-induced cell death, and rapid recovery of viscous properties to maintain print fidelity post-extrusion.[200] This imparts limitations

on the biofabrication window and the available chemical toolkit that exists for designing hydrogel-based bioinks and, as a consequence, for mimicking cellular microenvironments.

The rheological demands of extrusion-based requires bioink formulations to high polymer fractions, thereby limiting the use of more cell-permissive low polymer density bioinks. The concept of the "biofabrication window," introduced in 2013, describes balancing the cell-permissive nature of bioinks and the rheological profile required for extrusion-based bioprinting, and it has been a major focus of research in extrusion-based bioprinting since.[201] Viscosity modulators can be used to alter the flow properties during extrusion and/or affect shape recovery post extrusion.[202–205] Alternatively, controlling the timing of crosslinking can allow modulation of bioink printability. Ouyang et al. exposed a bioink to light while it was extruded through a transparent nozzle, initiating a partial crosslinking process and rendering the bioink printable before being fully crosslinking after printing.[206] Similarly, enzymatic crosslinking can be used prior to extrusion to increase the bioink viscosity, after which photo-initiated crosslinking post-fabrication can be applied to provide further shape stability.[207] The recent emergence of embedded bioprinting has also allowed the expansion of the biofabrication window. By printing bioinks into a bath of support material, that ensures shape retainment of the printed construct, bioink viscosity can be decoupled from shape retention capability, allowing the printing of low-viscous bioinks.[208] Jammed printing, wherein a bioink is composed of densely packed small pre-crosslinked microgels, is another method that enabled printing due to the attractive forces between the microgels that provides the ink with solid-like characteristics that can be made to print through applying pressure.[209] While these are all elegant strategies, each presents advantages and disadvantages for fabrication of constructs. The use of viscosity enhancers is limited as their inclusion affects not only the rheological profile of the bioink, but also the physical properties of the hydrogel. Consequently, it is challenging to simultaneously achieve adequate bioink printability and the formation of a tissue-specific and cell-instructive hydrogel. Light-based or enzymatic pre-crosslinking, as well as embedded bioprinting and jammed printing techniques, are technology-based approaches which require specialized equipment which currently limits their wide application. Sacrificial printing is an alternative strategy that circumvents the need of bioinks to adhere to the biofabrication window. This process involves the printing of a sacrificial template composed of cell-free or cell-laden sacrificial (bio)inks, the embedding of sacrificial templates within bulk hydrogels and finally the removal of the sacrificial template to leave open microchannels. The ability to engineer spatially defined microchannel structures within bulk hydrogels has gained interest within vascular tissue engineering, but it must be noted that this method provides limited opportunity to design spatial heterogeneity in the composition of the bulk hydrogel, thus hampering the ability to mimic the required micro- and macroscale arrangements of tissues surrounding the microchannels.[210]

5.1.1. Exploring Different Macromolecular Chemistry to Design Novel Bioinks

To date, a limited number of macromolecular chemistries have been utilized for extrusion-based bioprinting, with covalently crosslinked bioinks a primary focus (e.g., vinyl-based crosslinkable systems like Gel-MA in combination with viscosity enhancers such as gellan gum and collagen, and thiol-ene clickable systems such as allyl-functionalized gelatin).[14,118,119,197,203] Physical crosslinking has also been exploited in printable bioinks, such as ionically crosslinked alginate.[211–213] Despite the wide range of macromolecular chemistries available, a limited number of these chemistries have been translated to extrusion bioprinting which reduces the flexibility in tailoring the hydrogel microenvironment. Exploiting smart bioink crosslinking chemistry represents an additional, promising opportunity to expand the biofabrication window, achieving controlled biomimicry over both micro- and macroenvironment.

Bioinks with dynamic bonds can generate extrudable bioinks due to the rapidly reversible nature of bonds, which provide shear-thinning and self-healing properties.[95,214–216] Reversible shear-thinning was for instance observed in guest (adamantane)–host (β-cyclodextrin) HA bioinks that could be used for extrusion. This bioink was blended with methacrylated HA (HA-MA) to enable in situ crosslinking (i.e., photo-initiated crosslinking of the bioink through a transparent nozzle during extrusion) which in turn allowed multilayer printing (**Figure 5**A). Wang et al. synthesized aldehyde- and hydrazide-modified HA separately and combined them to allow the formation of hydrogels containing hydrazone (Schiff base) dynamic bonds.[215] Upon extrusion through the nozzle, the rapid bond breakage allowed the deposition of filaments, while the rapid bond recovery post-extrusion provided shape stability (Figure 5B).[215] Gradual (<10 min) self-healing then allowed associations to be formed between separately extruded biomaterials, which could be beneficial when printing multiple ink formulations.[215] To ensure long-term shape fidelity, a second photocrosslinkable interpenetrating network composed by HA-NOR was used for orthogonal photo-stiffening and photopatterning through a thiol-ene reaction with a thiol-containing rhodamine.[215]

Supramolecular bioinks possessing shear-thinning and self-healing properties have also been used for extrusion-based 3D printing applications.[217–220] Loebel et al. designed a supramolecular bioink made from a HA polymer backbone with grafted adamantane or β-cyclodextrin, which allowed crosslinks to form by guest–host interactions. The developed bioink had rapid self-healing capability and could be extruded with spatial control through extrusion-based 3D printing.[218] Due to the weak nature of dynamic and supramolecular bonds, constructs crosslinked purely through these types of bonds often demonstrate limited stacking and printed constructs often demonstrate limited shape and mechanical stability during culture. Further functionalization of the macromer with methacrylate group, permitted a secondary crosslinking step which aids in improving shape and mechanical stability in more complex 3D geometries.[218] In a similar approach, a dual crosslinking method was employed to 3D print a supramolecular hydrogel-based bioink composed by PEG-grafted chitosan, α-cyclodextrin and gelatin.[217] Primary crosslinking occurred through the aggregation of the pseudo-polyrotaxane-like side chains, which were formed from the host–guest interactions between α-cyclodextrin and PEG side chains, while the secondary crosslinking was mediated by the immersion of the construct in a solution containing β-glycerophosphate. Fibroblasts embedded in the bioink displayed high viability

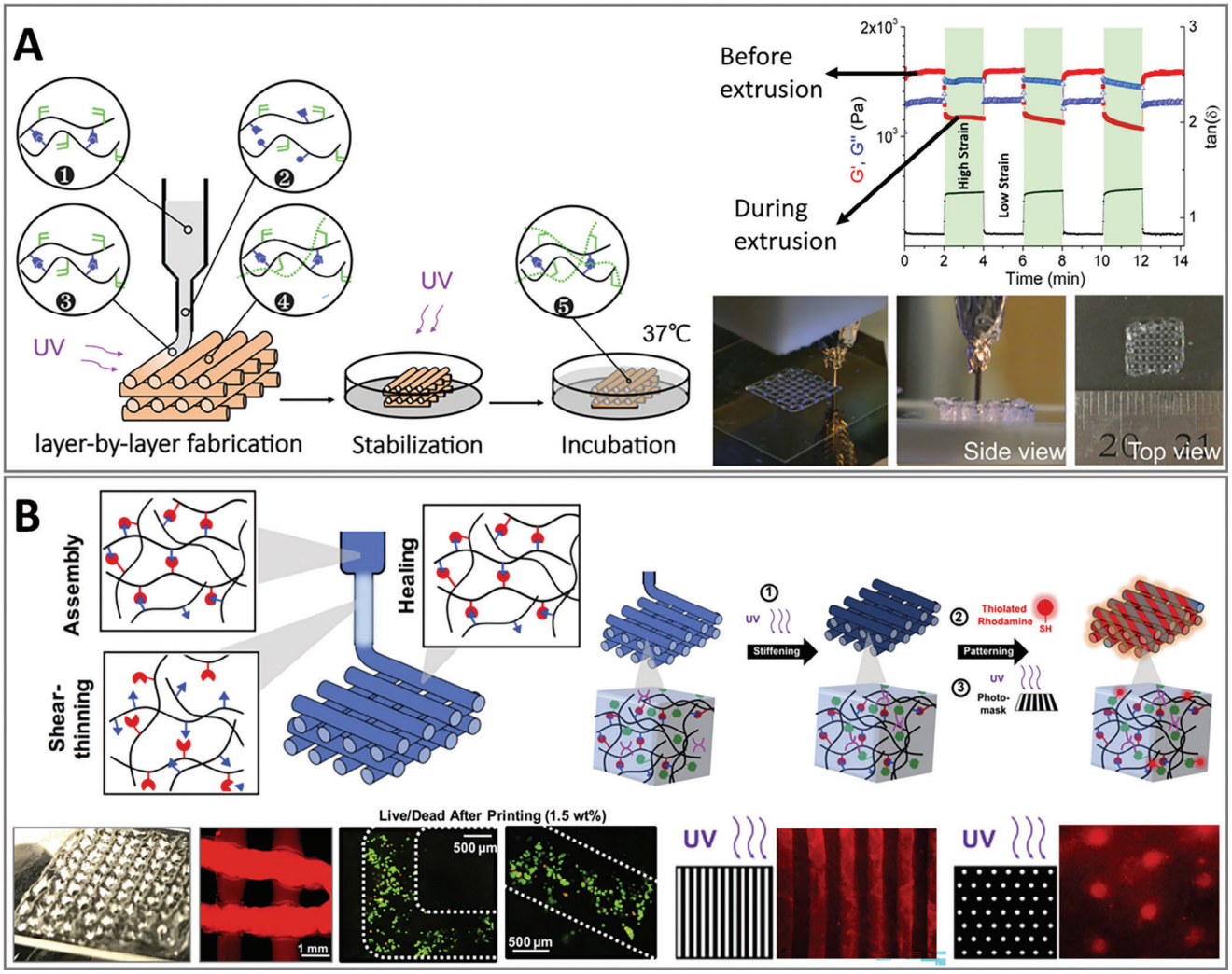

Figure 5. Dynamic and supramolecular hydrogels used in biofabrication. A) Printing of guest–host modified HA bioinks that demonstrated shear-thinning and self-healing (filament recovery) under multiple cycles of shear (simulating printing) without loss of bioink moduli. Reproduced with permission.[216] Copyright 2016, American Chemical Society. B) Rapid de-assembly of dynamic bonds in hydrazine/aldehyde-modified HA under shear stress, and self-healing properties allowed for extrusion of dynamic bioinks allowing printing, post-printing photocrosslinking for stiffening and photo-patterning. Reproduced with permission.[215] Copyright 2018, Wiley Periodicals, Inc.

after printing and increased proliferation and cadherin expression over time. Additionally, by tuning the β-glycerophosphate concentration, different stiffnesses could be achieved, which influenced MSCs differentiation.[217] The secondary photo- or enzymatically initiated crosslinking may be necessary to stabilize the weak dynamic and supramolecular bonds in printed constructs by introducing stable covalent bonds. Nevertheless, dual crosslinking could reduce the contribution of dynamic covalent bonds on bulk hydrogel characteristics, such as stimuli-responsivity and viscoelasticity, and the influence of dynamic bonds on cell behavior within printed constructs could be made redundant by the presence of stiffer covalent bonds. Thus, while tailoring the secondary crosslinking might represent a promising strategy to further tune the microenvironment and guide biological processes, this crosslinking interplay needs to be explored further.

5.2. Lithography-Based Bioprinting and Bioresin Properties

Stereolithographic bioprinting exploits light to cure a photosensitive resin (i.e., bioink specifically designed for lithography-based bioprinting), which typically contains a photo-initiator as well as reactive monomers and/or macromers (Figure 4A). By precisely exposing specific zones of the print area with the appropriate wavelength and intensity of light, resin crosslinking can be achieved with high spatial control (25–30 μm in resolution).[6,95] Light is introduced into the bioresin by using a laser (stereolithography; SLA), by projecting a light pattern onto the bioresin (digital light processing; DLP) or by a high-energy femtosecond laser (two-photon polymerization). Similar to extrusion-based bioprinting, there are distinct compatibility criteria for bioinks that can be used in lithography-based bioprinting, limiting the flexibility in the bioink design. The ideal bioresin should be of

low viscosity (0.25–10 Pa s) as a new volume of material needs to easily flow under the building platform after each layer is crosslinked, even in the absence of a mixing mechanism.[221] The high-resolution spatial control in lithography-based printing necessitates the prevention of unwanted crosslinking surrounding the point of light exposure and it is thus crucial to optimize the photocuring and light penetration depth.[6,222] Additionally, inherent light scattering during the crosslinking steps poses a significant challenge in forming high-fidelity structures with fine-scale features. To improve printability, bioresin formulations therefore often include photo-absorbers that are generally composed of food colorings such as Ponceau 4R. Novel photoinhibiting additives are also being developed in an attempt to widen the biofabrication window for lithography-based printing. In a recent example, He et al. showed that curcumin-Na could be used as a photoinhibiting complex, increasing the printing resolution and fidelity significantly and allowing the fabrication of complex constructs featuring intricate micro-sized channels and thin-walled networks.[223] Still, bioresin development generally requires extensive trial and error efforts to optimize both the printing parameters (e.g., light intensity) and bioink formulation (e.g., concentration of the different components) to achieve the desired fidelity for certain geometries.[224–226]

Compared to extrusion bioprinting, a key limitation with lithography-based printing is the challenges of processing of multiple bioresins within a singular printed construct, limiting the ability to create different microenvironment niches within constructs. Additionally, fabricating 3D constructs utilizing soft bioresins (i.e., polymer content < 10 wt%) has proved to be challenging, due to an insufficient integrity to retain shape upon moving of the collecting plate. Layer stacking can also be challenging in soft, low polymer content (<10 wt%) bioresins due to insufficient crosslinking at the layer interface, meaning that those reported are limited to patterned structures with no structural variation in the *Z*-axis.[227,228] As the fabrication of 3D geometries can be a lengthy process in SLA and DLP printing, depending on the constructs size, cell sedimentation in low viscosity bioresins represents another challenge.[229] To address it, advancements in bioresin design have seen the introduction of viscosity modulators, such as colloid polyvinylpyrrolidone-coated silica particles, which can induce neutral buoyancy to match the density between components in the bioink and allow cells to float in solution.[230] While this approach successfully reduces cell sedimentation, it also induces unwanted crosslinking and therefore consideration of the final application (i.e., the resolution required for mimicking relevant features of the target tissue) is necessary when designing bioinks for lithography-based bioprinting.

The development of volumetric bioprinting, a novel light-based printing method where whole objects are generated in a layerless fashion, allows the printing of clinically relevant sized constructs possessing complex architectures within seconds. This speed overcomes the challenges associated with cell sedimentation without compromising the printing resolution, and allows the precise imprinting of biochemical or biophysical cues in specific areas of large 3D constructs, creating heterogeneous microenvironments which can direct cell behavior.[231–233] Falandt et al. exploited this technology to spatially pattern VEGF-rich areas within a centimeter-scale, thiol-ene photo-crosslinkable 5 wt% Gel-NOR bioresin.[234] By exploiting thiol-ene chemistry, accurate control over the crosslinking kinetics and reaction termination upon removal of light irradiation could be achieved, making it possible to contextually control the amount of unreacted norbornene groups. These unreacted groups were exploited for a secondary reaction, which allowed VEGF conjugation which promoted endothelial cell migration and a higher number of vascular junctions.[234]

5.3. Microfluidic-Driven Biofabrication for Complex Microenvironment Design

Microfluidics is a widely used technique focusing on the controlled introduction and combination of multiple fluids within micro- to millimeter-sized channels. The geometric constraints of these channels create an environment in which the material's rheological properties (e.g., viscosity and surface tension) affect fluid flow more than gravitational forces, which often affects laminar flow when introducing multiple fluids within a channel.[235] Microfluidics can be used for the fabrication of cell-laden hydrogels with well-defined physical properties, as well as hydrogels with complex spatial arrangements due to the well-defined fluid flow regimes that exist within the microfluidics channels (**Table 2**).[236] This level of complexity can be achieved by introducing multiple hydrogel precursor solutions in laminar flow within microfluidic channels, prior to crosslinking of the hydrogels through ionic crosslinking or photo-initiated crosslinking.

Microfluidics has been merged within top-down biofabrication techniques to generate spatial control of engineered microenvironments (Figure 4A). The majority of these approaches implement various microfluidics chip designs into printhead design in extrusion-based printing. By controlling the flow of various fluid phases into a singular printhead, thereby exploiting the microscale control provided through microfluidics, simultaneous control over the tissue microenvironment and macroscale construct geometry is possible. Co-axial printheads provide a promising microfluidics-assisted printing platform, whereby two or more concentrically orientated fluids are introduced into a singular outlet in laminar flow.[244] These flow patterns result in a core-sheet morphology, allowing diffusion-driven movement of molecules across the fluid interface. By tailoring the compositions of each of these fluids, smart use of macromolecular chemistry in combination with co-axial printheads has resulted in several notable advancements, including the printing of otherwise unprintable bioinks. Low-viscous alginate bioinks can be printed as the alginate and calcium chloride ($CaCl_2$) phases meet in the tip of the co-axial needle whereby crosslinking occurs, allowing the deposition of high shape fidelity alginate filaments without the use of a support bath. This approach has been used to fabricate alginate-based cartilage bioinks[245] and various other photo-polymerizable biomaterials. Alginate has also been combined with other bioinks to form printable hybrid bioinks.[246,247] For instance, low polymer density Gel-MA and alginate have been combined in core fluid flow, with the core including a UV-sensitive photo-initiator to allow photo-polymerization and the sheath flow containing $CaCl_2$.[246,247] While otherwise unprintable, rapid $CaCl_2$-mediated ionic crosslinking of alginate at the nozzle tip provides extruded bioinks with sufficient structural integrity to enable the stacking of printed filaments, after which UV

Table 2. Overview of various designs for multiphasic cell-laden patterned filaments. Endothelial cell; EC, fibroblast; FB, gelatin-methacryloyl; Gel-MA, human umbilical vein endothelial cell (HUVEC), poly(ethylene glycol); PEG, poly(ethylene glycol)-diacrylate; PEG-DA).

Schematic	Component A	Component B	Outcome	Ref
	Alginate + glioma stem cells	Glioma cell line	Mimicry native glioma cell orientation	[237]
	2% alginate + FBs	2% alginate + HUVECs	Biomimicry blood vessel, functional output lacking	[238]
	4% alginate + 0.8% PEG-fibrinogen + C2C12 cells	4% alginate + 0.8% PEG-fibrinogen + FBs	Proof-of-concept Janus with cells	[239]
	3% collagen + HepG2 cells	3% collagen + ECs	Biomimicry hepatic lobe	[240]
	7% Gel-MA + 2% alginate + 2% PEG-DA + C2C12 cells	7%s Gel-MA + 2% alginate + 2% PEG-DA + FBs	Cytocompatibility cells in hollow bilayer tubes	[241]
	2% alginate	3% Gel-MA + 1% alginate + C2C12 cells		[242, 243]

photo-polymerization induced Gel-MA crosslinking permits the formation of a construct that was stable during culture at physiological conditions. When human umbilical vein endothelial cells (HUVECs) were incorporated into the hybrid bioink, lattice structures could be printed which showed cell migration to the exterior of the construct filaments to form an endothelium.[246] Multiple bioink formulations can also be used in the sheath of the co-axial filaments to fabricate filaments in rings of spatially patterned anisotropy, and sacrificial inks can be used within a multi-material setting to create hollow regions within a filament upon sacrificial ink dissolution. Using Pluronics F-127 as a sacrificial ink in the filament core and endothelial progenitor cell-laden bioinks in the outer layer, hollow filaments can be printed that support endothelialization of the internal and external filament surfaces over 7 days of culture.[248] Anisotropic environments have been created within alginate (core) and collagen (shell) filaments in printed lattice structures.[249] The alginate and collagen areas were clearly distinguishable through scanning electron microscopy, with the recorded stiffness of alginate and collagen at 11.2 and 1.32 MPa, respectively prior to filament generation. Cells can also be spatially compartmentalized in core–shell alginate bioinks to better mimic the tumor microenvironments.[237]

Hollow filaments can be extruded with walls composed of alternating single- or double-layered biomaterials by switching the feeding of the singular material or both materials, respectively (**Figure** 6A). These filaments were used to pattern HUVECs in the inner sheath, while smooth muscle cells were encapsulated in the outer sheath, demonstrating endothelium formation over a period of 14 days.[250] Nevertheless, the effects of varying the one- and two-layered filament wall across the filament length has not been investigated. While most co-axial printheads use circular sheaths, other shapes can be used to further adjust the spatial patterns of separate bioinks.[240] By increasing the number of feeds into the printhead, this technique can be expanded to include three[251] or even seven[241] separate bioinks with smooth transitions between bioinks in extruded filaments. Using this technique, discrete regions can be fabricated by varying HA concentrations within hydrogel discs or sheets.[241] Native blood vessel architecture can be mimicked by creating cell-laden, two-layered filaments, with a HUVEC-laden inner sheath and fibroblast-laden outer sheath.[238] While fibroblasts migrated into the inner HUVEC-laden sheath, collagen and fibrin were required within the inner sheath to encourage HUVEC growth.[238] The authors also demonstrated proof-of-concept for generating more complex microenvironments through the formation of tri-layer hollow filaments using sequential introduction of alginate bioinks, albeit without the inclusion of cells. These strategies illustrate the potential of compartmentalizing cells in multi-layered filaments, but also highlights the importance of optimizing bioink formulations for specific applications.

In another type of strategy, two separate bioinks can be combined using a simple Y-shape channel to fabricate a Janus-like filaments. In one example, bioinks composed of Gel-MA/alginate were combined in this way and subsequently fed into a co-axial needle with an introduced laminar $CaCl_2$ flow to crosslink the filament.[239,253] By varying which bioink is printed during fabrication, multi-layered constructs with alternating layers of the two bioinks could be fabricated from the singular co-axial needle (Figure 6B).[253–255] A similar setup was used in combination with a microfluidic mixer to generate gradient structures. In this system, the relative flow rate of two alginate-based bioinks was varied during the printing process wherein the microfluidic mixer enabled mixing of the two inks in flow rate-defined ratios prior to extrusion through the co-axial nozzle (Figure 6C).[12]

Rather than homogeneously mixing inks, partial chaotic mixing can be used to form unique patterns within bioinks.[242,243] Sequential static mixer elements have been used to mix two bioinks, creating a chaotic pattern within the filament cross-section. Using alginate/graphite bioinks, 35–500 µm striations could be patterned within the filaments, which in turn could be printed into

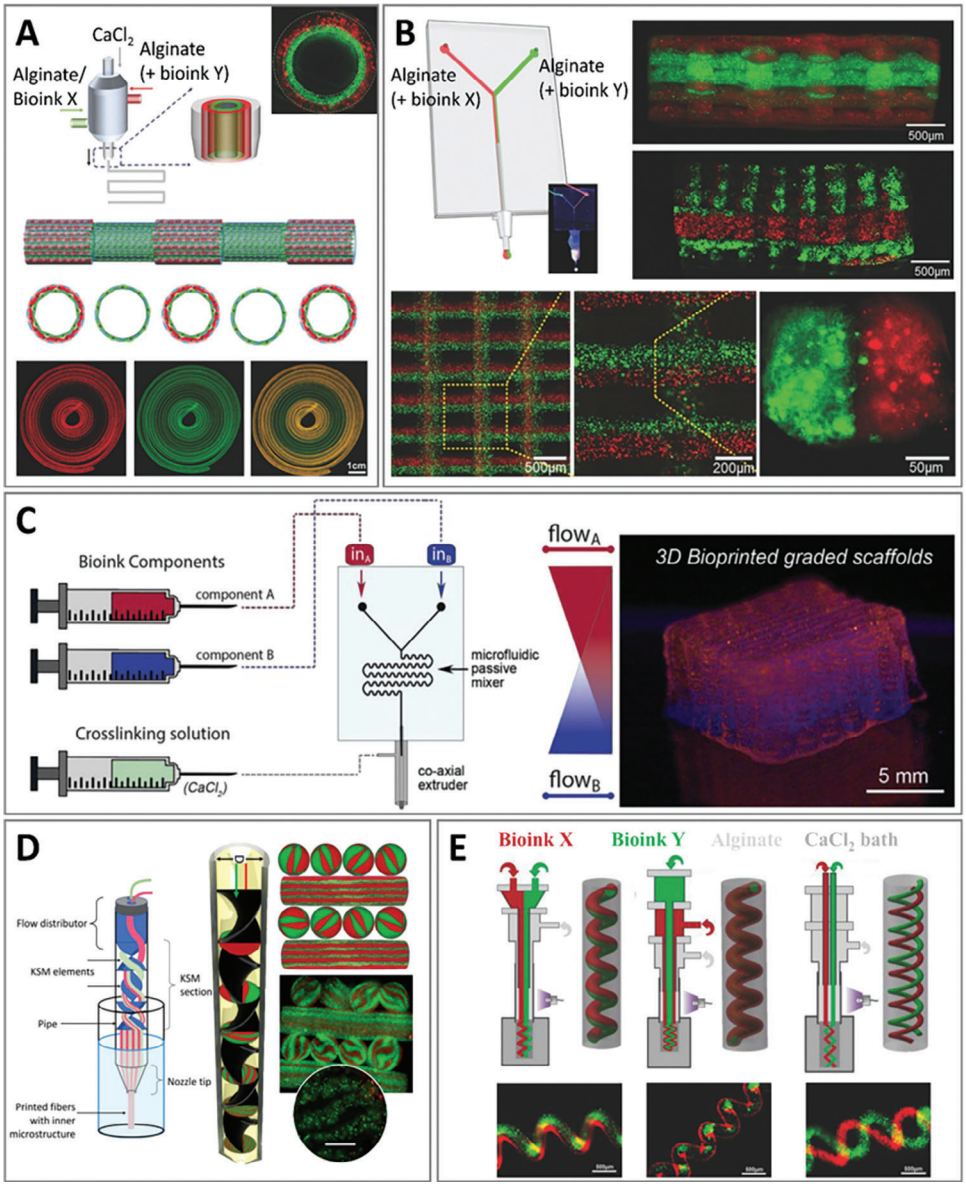

Figure 6. Co-axial and microfluidics-based printing of multiphasic cell-laden filaments. A) Introduction of alginate-based bioinks or blend bioinks including alginate in co-axial flow. Control of bioink flow regimes allowed for smooth switching of single- and bi-layered hollow filaments. Reproduced with permission.[250] Copyright 2018, WILEY-VCH Verlag GmbH & Co. KGaA, Weinheim. B) Introduction of alginate-based bioinks through Y-shaped channels followed by co-axial introduction of $CaCl_2$ prior to printing. Reproduced with permission.[239] Copyright 2015, WILEY-VCH Verlag GmbH & Co. KGaA, Weinheim. C) Microfluidics-assisted efficient mixing of two bioinks within a microfluidic mixer to generate gradient printed scaffolds. Reproduced with permission.[12] Copyright 2019, IOP Publishing, Ltd. D) Partial mixing of two bioinks can lead to chaotic bioink patterns within biofabricated constructs. Reproduced under the terms of the Creative Commons CC-BY 4.0 License.[242] Copyright 2020, The Authors(s). Published by IOP Publishing Ltd. E) In situ crosslinking of photo-polymerizable bioinks in laminar flow. Printing of helical structures of photo-polymerized bioinks within alginate sheaths, owing to the flow rate differences between alginate and bioink phases after in situ crosslinking. Reproduced with permission.[252] Copyright 2018, WILEY-VCH Verlag GmbH & Co. KGaA, Weinheim.

lattice macrostructures (Figure 6D). With cell-encapsulation, addition of Gel-MA into one of the two bioinks resulted in filament striations with evidence of cell spreading.[242] Evidently, microfluidics-driven extrusion-based printing provides a promising opportunity for improved spatial patterning of biophysical cues, whilst also allowing spatial control over the physical architecture of fabricated constructs. However, developments have been highly technology-focused and most reports have utilized rapid ionic crosslinking in alginate prior to extrusion. This highlights a clear area for further development: expanding the library of biomaterial which are compatible with microfluidics-assisted printing. In situ photo-crosslinking (i.e., exposing biomaterials to light during extrusion) is one strategy to achieve this in microfluidics-assisted printing (Figure 6E), enabling printing of a range of materials including PEG-diacrylate, HA-MA, HA-NOR and Gel-MA.[206] However, in situ crosslinking of the core

biomaterial can alter the viscosity of inks, leading to altered flow speed of the core and sheath phases and coiling of the core biomaterial. This has been exploited to fabricate helical filaments,[252] which have then further been incorporated within larger filaments.[254] In the wider scope of biofabrication, the convergence of microfluidics and other biofabrication platforms might provide an alternative avenue toward expanding the macromolecular toolkit for bioink design. To exemplify, microfluidics has been combined with lithograph-based bioprinting to allow multi-material light-based patterning of photopolymerizable bioinks. Bioinks were introduced within the microfluidics chip chamber and exposed to defined light patterns before rapidly (<5 s) washing away the bioink to allow inflow of the next bioink.[256] More recently, microfluidic mixers have also been incorporated within the microfluidic-driven lithography-based printing approach to enable the formation of well-defined multi-material, cellular, growth factor, stiffness and porosity gradient.[257] Areas of future work in microfluidics-driven biofabrication should be directed toward understanding the biological effects of spatially patterning cells, multiple bioinks and spatial-patterning of inks through chaotic mixing. By adjusting the formulations of these various bioinks, it could be possible to pattern different regions within filaments to provide cell-specific niches. For example, multi-layered filaments could incorporate tissue microenvironments conducive to formation of native tunica intima, media and externa for blood vessel formation. Similarly, the multiple layer gradients present in cartilage and subchondral bone could be reproduced by optimizing bioink mixing and by varying cell concentrations throughout printing.

6. Temporal Control over Physico-Chemical Cues within the Micro- and Macro-Environment

Native tissue formation, maturation and homeostasis are complex processes whereby the physical properties vary throughout tissues, as well as vary dynamically during these processes. Biofabrication platforms, such as extrusion-based 3D printing, are predominantly used to spatially pattern inks to generate specific physical architectures; however they also allow temporal control over the presentation of biophysical cues within cell-laden hydrogels and tissue substitutes. Four-dimensional (4D) printing, a subsection of 3D printing, involves temporally controlled manipulation of construct shape post fabrication.[95,258,259] These printed materials undergo changes alongside variations in external stimuli that are introduced with temporal control, such as temperature[260] and magnetic fields that affect their shape.[261] The majority of 4D printable inks however are not compatible with cells. The operating window of these external cues are for instance often outside of the window compatible with cell culture conditions. In addition, 4D printable inks often need to be printed at high temperatures which are not cell permissive. Consequently, identifying 4D printing methods that are compatible with physiological temperature, humidity and pH, to allow the incorporation of cells within these constructs, will be vital for the development of this technology.

There has been progression in the development of 4D bioinks that can operate at physiological conditions (i.e., conditions that could be compatible with the introduction of cells). These approaches generally involve blending multiple inks that swell to varying degrees, wherein macroscale temporal structural changes are driven by anisotropic swelling of the printed constructs that leads to folding of the printed structures. In an example, nanofibrillated cellulose was combined with *N*-isopropylacrylamide (NIPAm). Extrusion-induced shear stress causes cellulose fibril alignment and this fibril arrangement is subsequently preserved upon NIPAm photo-polymerization. The cellulose alignment along the extruded filaments results in anisotropic swelling which can be used to fabricate intricate 3D architectures.[262] Simple multi-layered hydrogel sheets can be also be generated through photolithography, involving 4D fabrication of a bottom layer that swells and folds in response to changes in pH[263] or temperature.[264] As the top sheet does not fold, the bottom sheet folds into a bilayer tube and if a sacrificial material is used as the top layer, the pH or temperature-induced generation of hollow tubes is possible. Furthermore, nano-topological features can be patterned on the inside of the tubes by using soft lithography stamps to pattern structures onto the layer prior to folding. An MSC-encapsulated methacrylated alginate and HA blend bioink was printed into filaments, which self-folded into tubes due to the presence of a crosslinking gradient from light attenuation. The softer, deeper areas of the bioink swelled more due to the lower crosslinking density. This folding technique is particularly attractive due to the size of the tube inner diameters, which can be made smaller than with conventional 3D printing, with outer and inner diameters as small as 200 and 20 µm, respectively.[265] Near-infrared (NIR) light can also be used to induce folding of polydopamine/alginate blends, as NIR-light absorbance of polydopamine causes dehydration. This attribute can be exploited to cause shrinkage of polydopamine/alginate regions, resulting in folding of those areas. This material blend has been used within extrusion-based printing, wherein spatial enabled the spatial patterning of folding polydopamine/alginate regions with unfolding Gel-MA/alginate regions, containing encapsulated embryonic kidney cells, resulted in light-sensitive shape-changing structures.[266]

Supramolecular bioinks may be well-suited as stimuli-sensitive hydrogels for 4D printing as inks that respond to external cues, e.g. pH, temperature, electricity, mechanical, and light. pH-sensitive hydrogels are commonly used as drug-delivery vehicles, exploiting (de)protonation of acrylic and methacrylic acid linkers, and exploiting the natural pH-sensitivity of biomaterials (e.g., chondroitin sulfate,[267] peptide amphiphiles and ureidopyrimidinone guest–host interactions[268]) to induce changes in hydrogel equilibrium swelling.[269] While cell-laden hydrogels are limited to a narrow pH range, local or bulk pH changes can still be leveraged within tissue engineering.[270] Other stimuli which have been exploited include temperature (e.g., in the context of sacrificial printing), electricity[271] (e.g., to make conductive hydrogels), magnetic fields and mechanically responsive hydrogels.[272] While viscoelastic hydrogels are inherently mechanically responsive, due to processes such as stress relaxation, incorporation of mechanoresponsive molecules can provide further spatial control. PEG-MA crosslinked with methacrylated di-hydrolipoic acid allows the formation of hydrogels that responded to strain by forming disulfide bond links between lipoic acid residues.[273] Light-sensitive hydrogels are especially interesting within 4D printing, as they provide further spatial control over hydrogel properties. A

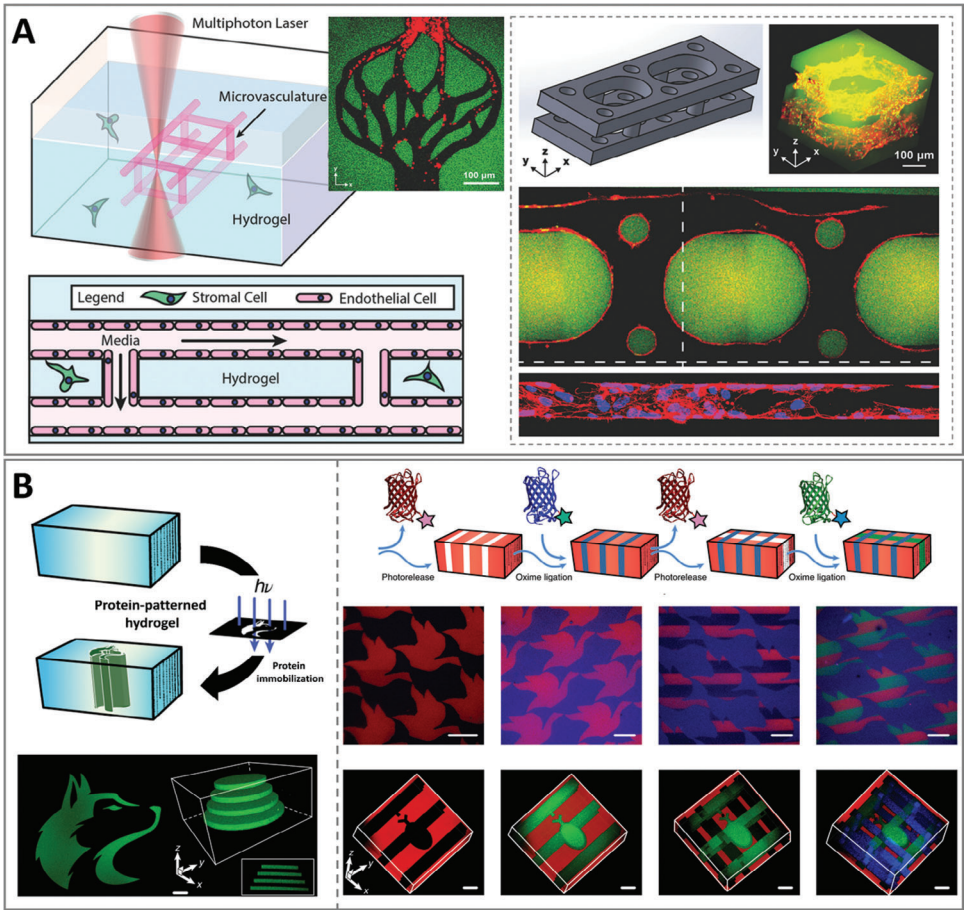

Figure 7. Light-responsive patterning in 3D hydrogel structures. A) Multiphoton patterning of open lumen within MSC-laden PEG hydrogels that are subsequently seeded with HUVECs. Endothelialization (red) of hydrogels (green) is observed and endothelization is partially observed (F-actin). Reproduced with permission.[281] Copyright 2017, WILEY-VCH Verlag GmbH & Co. KGaA, Weinheim. B) Sequential grafting of proteins with red, green and blue fluorescent tags by repetitions of photopatterning process; proteins are grafted to PEG hydrogel through oxime ligation, and then removed in parts of the constructs by further light exposure. Reproduced with permission.[282] Copyright 2019, The Author(s), under exclusive license to Springer Nature Limited.

common strategy involves the incorporation of light-sensitive moieties, such as fumaric amide,[274] dithienylethene tripeptide,[275] azobenzene,[276] coumarin[277] and ortho-nitrobenzyl (O-NB). These photo-responsive molecules can be used as photodegradable linkers.[278] O-NB was used to uncage alokxyamines on a PEG-peptide hydrogel, which subsequently reacted with aldehyde-modified proteins in solution. By spatially controlling light exposure, vitronectin can be grafted onto the polymer backbone, promoting osteogenesis within these exposed regions.[279] Aldehyde-modified multi-arm crosslinkers have been photo-patterned to increase local hydrogel stiffness,[280] generate open channels within hydrogels through multiphoton photodegradation (**Figure** 7A),[281] and sequential reversible protein binding (Figure 7B).[282] Reversible protein binding allowed continuous protein gradients to be patterned into hydrogels dynamically during cultivation. Dynamic hydrogels have also been generated by incorporating coumarin (guest) and cucurbit (host). Upon light exposure, coumarin dimers can be generated which increase hydrogel stiffness and switch the hydrogel phenotype to a covalently crosslinked hydrogel.[277] To improve the temporal control provided by biofabrication techniques, future work should be directed at further incorporation of stimuli-sensitive motifs within bioinks.

While some advancements have been made toward achieving temporal control over the presentation of biophysical cues within printable (i.e., cell-free) inks, the temporal control that can be achieved for cell-laden bioinks is limited. This is surprising given that spatiotemporal control is one of the main pillars of biofabrication. Further development of biofabrication platforms which enable both spatial control over the presentation of biophysical cues in cell-laden hydrogels and also temporal control over the presentation of such cues is necessary. Harnessing sophisticated macromolecular chemistries (e.g., for the incorporation of stimuli-sensitive motifs) is a promising path to achieving this goal. Overall, biofabrication platforms have enabled the spatiotemporal control over the placement of cell-laden hydrogels to varying degrees. There are clear challenges of the resolution scales at which popular biofabrication platforms operate (i.e., 20–200 μm), which are insufficient to enable adequate spatiotemporal control over the presentation of biophysical cues within the

direct micro-environment of encapsulated cells. Therefore, controlling the physical properties of the bioinks themselves by harnessing macromolecular chemistry is crucial for the fabrication of tissue substitutes that adequately mimic the multi-scale complexity of native tissues.

7. Translational Considerations

Engineering constructs that replicate specific physical properties from native tissues has proven to be effective in tailoring cell behavior in vitro.[3,283] However, it is still unknown to which properties of native tissue, and to what degree they need to be mimicked, to achieve successful regeneration in vivo. Mechanisms through which biomimetic cues affect in vitro cell migration, proliferation and differentiation has been investigated,[3] however the translation of these findings to in vivo models is difficult. While biological effects are commonly observed in well-controlled in vitro models with only a few variables present, these same findings may not always translate to more complex in vivo models where more variables are present. For instance, the relevance of durotactic effects in predicting or affecting cell behavior in vivo is still under debate.[59,284] Moreover, while biomimetic tissue substitutes are generally developed to mimic the properties of native tissues under physiological conditions,[13] these engineered constructs are usually implanted at injured sites undergoing wound healing events.[13,285] This may trigger different biological effects from what was predicted. Exploring the targeted cellular response to hydrogel physico-chemical cues during the wound healing cascade, such as the introduction of immune cells and an inflammatory response, is a valuable area of research.[285,286]

A key consideration for preclinical translation of engineered constructs is the appropriate selection of in vivo model. Ectopic models provide valid information about biocompatibility and, to some extent, the capability of the constructs to induce new tissue formation.[287,288] Nevertheless, since the microenvironment of tissue substitutes has been tailored to match the unique characteristics of a specific host tissue, and to trigger effects on specific host resident cells, it is crucial to evaluate the regeneration induced in orthotopic models.[287,288] Increasing complexity in the rational design of micro- and macro-environments needs to be critically evaluated to ensure there is a benefit from a biological perspective.[289] It is important to define whether increased design complexity, fabrication time, costs and post-fabrication modifications significantly enhance tissue regeneration compared with simpler strategies, as this influences the clinical feasibility of engineered tissue substitutes.[289,290] Similarly, the dynamic nature of tissue maturation, and the benefit of mimicry of these dynamics through temporal control over the micro- and macro-environments of engineered tissues, should be considered.

8. Conclusions

Native tissue microenvironments are characterized by their specific physico-chemical properties which drive tissue function. There has been a huge body of work focused on exploiting macromolecular chemistry for the rational design of hydrogels that mimic specific properties of the native microenvironment, to promote tissue regeneration. Nevertheless, there is still no consensus on which native properties are essential in order to trigger specific biological responses. As the physico-chemical properties of hydrogels (i.e., crosslinking density, mesh size, pore size, porosity, and stiffness) are interrelated, it is challenging to systematically investigate the effect of individual parameters on cell behavior. Future work should focus more comprehensively on harnessing macromolecular chemistry to allow the decoupling of individual biophysical and chemical cues, to identify those that are essential for designing biomimetic and regenerative tissue constructs. Additionally, generating complex microenvironments with multiple cues distributed in a controlled fashion will allow conclusions to be formed on their hierarchical relevance. Combining the identified key physico-chemical cues present in the microenvironment, with a biomimetic macroenvironment represents a promising strategy for the successful tissue regeneration.

Acknowledgements

B.G.S. and A.L. contributed equally to this work. The authors would like to acknowledge funding support from the Health Research Council of New Zealand (Sir Charles Hercus Health Research Fellowship 19/135, Project Grant 20/508), Royal Society Te Apārangi (Marsden Fast Start Grant MFP-UOO1826), NSW Health (H22/98586), and Australian Research Council (FT230100249).

Open access publishing facilitated by The University of Sydney, as part of the Wiley - The University of Sydney agreement via the Council of Australian University Librarians.

Conflict of Interest

The authors declare no conflict of interest.

Keywords

biofabrication, biomimcry, hydrogels, macromolecular chemistry, tissue engineering

Received: October 7, 2023
Revised: November 16, 2023
Published online: December 20, 2023

[1] C. A. Vacanti, *J. Cell. Mol. Med.* **2006**, *10*, 569.
[2] D. E. Ingber, V. C. Mow, D. Butler, L. Niklason, J. Huard, J. Mao, I. Yannas, D. Kaplan, G. Vunjak-Novakovic, *Tissue Eng.* **2006**, *12*, 3265.
[3] G. Huang, F. Li, X. Zhao, Y. Ma, Y. Li, M. Lin, G. Jin, T. J. Lu, G. M. Genin, F. Xu, *Chem. Rev.* **2017**, *117*, 12764.
[4] H. Atcha, Y. S Choi, O. Chaudhuri, A. J. Engler, *Cell Stem Cell* **2023**, *30*, 750.
[5] I. Calejo, R. Costa-Almeida, R. L. Reis, M. E. Gomes, *Trends Biotechnol.* **2020**, *38*, 83.
[6] K. S. Lim, J. H. Galarraga, X. Cui, G. C. J. Lindberg, J. A. Burdick, T. B. F. Woodfield, *Chem. Rev.* **2020**, *120*, 10662.
[7] Y. S Zhang, A. Khademhosseini, *Science* **2017**, *356*, 3627.
[8] N. Eslahi, M. Abdorahim, A. Simchi, *Biomacromolecules* **2016**, *17*, 3441.
[9] Q. Wei, J. Young, A. Holle, J. Li, K. Bieback, G. Inman, J. P. Spatz, E. A. Cavalcanti-Adam, *ACS Biomater. Sci. Eng.* **2020**, *6*, 4687.
[10] B. G. Soliman, G. S. Major, P. Atienza-Roca, C. A. Murphy, A. Longoni, C. R. Alcala-Orozco, J. Rnjak-Kovacina, D. Gawlitta, T. B. F. Woodfield, K. S. Lim, *Adv. Healthcare Mater.* **2022**, *11*, e2101873.

[11] N. Mehrban, B. Zhu, F. Tamagnini, F. I. Young, A. Wasmuth, K. L. Hudson, A. R. Thomson, M. A. Birchall, A. D. Randall, B. Song, D. N. Woolfson, *ACS Biomater. Sci. Eng.* **2015**, *1*, 431.
[12] J. Idaszek, M. Costantini, T. A. Karlsen, J. Jaroszewicz, C. Colosi, S. Testa, E. Fornetti, S. Bernardini, M. Seta, K. Kasarello, R. Wrzesien, S. Cannata, A. Barbetta, C. Gargioli, J. E. Brinchman, W. Swieszkowski, *Biofabrication* **2019**, *11*, 044101.
[13] G. Zhu, T. Zhang, M. Chen, K. Yao, X. Huang, B. Zhang, Y. Li, J. Liu, Y. Wang, Z. Zhao, *Bioact. Mater.* **2021**, *6*, 4110.
[14] B. G. Soliman, A. Longoni, M. Wang, W. Li, P. N. Bernal, A. Cianciosi, G. C. J. Lindberg, J. Malda, J. Groll, T. Jungst, R. Levato, J. Rnjak-Kovacina, T. B. F. Woodfield, Y. S Zhang, K. S. Lim, *Adv. Funct. Mater.* **2023**, *33*, 2210521.
[15] Y. Wang, R. K. Kankala, C. Ou, A. Chen, Z. Yang, *Bioact. Mater.* **2022**, *9*, 198.
[16] P. Madhusudanan, G. Raju, S. Shankarappa, *J. R. Soc., Interface* **2020**, *17*, 20190505.
[17] B. J. Klotz, L. A. Oosterhoff, L. Utomo, K. S. Lim, Q. Vallmajo-Martin, H. Clevers, T. B. F. Woodfield, A. J. W. P. Rosenberg, J. Malda, M. Ehrbar, B. Spee, D. Gawlitta, *Adv. Healthcare Mater.* **2019**, *8*, e1900979.
[18] S. Anil Kumar, M. Alonzo, S. C. Allen, L. Abelseth, V. Thakur, J. Akimoto, Y. Ito, S. M. Willerth, L. Suggs, M. Chattopadhyay, B. Joddar, *ACS Biomater. Sci. Eng.* **2019**, *5*, 4551.
[19] A. J. Sophia Fox, A. Bedi, S. A. Rodeo, *Sports Health* **2009**, *1*, 461.
[20] M. Hirao, J. Hashimoto, N. Yamasaki, W. Ando, H. Tsuboi, A. Myoui, H. Yoshikawa, *J. Bone Miner. Metab.* **2007**, *25*, 266.
[21] S. Ansari, S. Khorshidi, A. Karkhaneh, *Acta Biomater.* **2019**, *87*, 41.
[22] E. F. Morgan, G. U. Unnikrisnan, A. I. Hussein, *Annu. Rev. Biomed. Eng.* **2018**, *20*, 119.
[23] L.-C. Gerhardt, A. R. Boccaccini, *Materialss* **2010**, *3*, 3867.
[24] F. Boschetti, M. Colombo, G. Peretti, G. Fraschini, R. Pietrabissa, *Trans. Annu. Meet. - Orthop. Res. Soc.* **2003**, *28*, 293.
[25] J. E. Wagenseil, R. P. Mecham, *Physiol. Rev.* **2009**, *89*, 957.
[26] G. Bou-Gharios, M. Ponticos, V. Rajkumar, D. Abraham, *Cell Proliferation* **2004**, *37*, 207.
[27] J. M. Muncie, V. M. Weaver, *Curr. Top. Dev. Biol.* **2018**, *130*, 1.
[28] A. Sainio, H. Järveläinen, *Cell. Signal.* **2020**, *66*, 1109487.
[29] A. Longoni, L. Knezevic, K. Schepers, H. Weinans, A. J. W. P. Rosenberg, D. Gawlitta, *NPJ Regener. Med.* **2018**, *3*, 22.
[30] J. Li, Y. Liu, Y. Zhang, B. Yao, Enhejirigala, Z. Li, W. Song, Y. Wang, X. Duan, X. Yuan, X. Fu, S. Huang, *Front. Cell Dev. Biol.* **2021**, *9*, 640388.
[31] R. C. H. Gresham, C. S. Bahney, J. K. Leach, *Bioact. Mater.* **2021**, *6*, 1945.
[32] K. Forsten-Williams, C. L. Chu, M. Fannon, J. A. Buczek-Thomas, M. A. Nugent, *Ann. Biomed. Eng.* **2008**, *36*, 2134.
[33] O. Nilsson, E. A. Parker, A. Hegde, M. Chau, K. M. Barnes, J. Baron, *J. Endocrinol.* **2007**, *193*, 75.
[34] P. Garrison, S. Yue, J. Hanson, J. Baron, J. C. Lui, *PLoS One* **2017**, *12*, e0176752.
[35] F. Mac Gabhann, J. W. Ji, A. S. Popel, *J. Appl. Physiol.* **2007**, *102*, 722.
[36] L. Liu, B. D. Ratner, E. H Sage, S. Jiang, *Langmuir* **2007**, *23*, 11168.
[37] P. Bao, A. Kodra, M. Tomic-Canic, M. S. Golinko, H. P Ehrlich, H. Brem, *J. Surg. Res.* **2009**, *153*, 347.
[38] D. Rodriguez, D. Watts, D. Gaete, S. Sormendi, B. Wielockx, *Int. J. Mol. Sci.* **2021**, *22*, 9191.
[39] T.-J. Cho, L. C. Gerstenfeld, T. A. Einhorn, *J. Bone Miner. Res.* **2002**, *17*, 513.
[40] M. Lockhart, E. Wirrig, A. Phelps, A. Wessels, *Birth Defects Res., Part A* **2011**, *91*, 535.
[41] E. D. Carruth, A. D. Mcculloch, J. H. Omens, *Prog. Biophys. Mol. Biol.* **2016**, *122*, 215.
[42] R. Mcclelland, E. Wauthier, J. Uronis, L. Reid, *Tissue Eng., Part A* **2008**, *14*, 59.
[43] M. N. George, X. Liu, A. L. Miller, H. Xu, L. Lu, *J. Biomed. Mater. Res., Part A* **2020**, *108*, 515.
[44] A. A. Reszka, J. M. Halasy-Nagy, P. J. Masarachia, G. A. Rodan, *J. Biol. Chem.* **1999**, *274*, 34967.
[45] K. Stamati, V. Mudera, U. Cheema, *J. Tissue Eng.* **2011**, *2*, 204173141143236.
[46] D. K. Taheem, G. Jell, E. Gentleman, *Tissue Eng., Part B* **2020**, *26*, 105.
[47] A. Zimna, M. Kurpisz, *Biomed. Res. Int.* **2015**, *2015*, 549412.
[48] Y. Liu, S. R. Cox, T. Morita, S. Kourembanas, *Circ. Res.* **1995**, *77*, 638.
[49] T. Lang, A. Leblanc, H. Evans, Y. Lu, H. Genant, A. Yu, *J. Bone Miner. Res.* **2004**, *19*, 1006.
[50] B. Vanwanseele, F. Eckstein, H. Knecht, A. Spaepen, E. Stüssi, *Arthritis Rheum.* **2003**, *48*, 3377.
[51] R. C. Entwistle, S. C. Sammons, R. F. Bigley, S. J. Hazelwood, D. P. Fyhrie, J. C. Gibeling, S. M. Stover, *J. Orthop. Res.* **2009**, *27*, 1272.
[52] B. R. Mandelbaum, J. E. Browne, F. Fu, L. Micheli, J. B Mosely, C. Erggelet, T. Minas, L. Peterson, *Am. J. Sports Med.* **1998**, *26*, 853.
[53] K. Dey, E. Roca, G. Ramorino, L. Sartore, *Biomater. Sci.* **2020**, *8*, 7033.
[54] H. Yokota, D. J. Leong, H. B. Sun, *Curr. Osteoporos. Rep.* **2011**, *9*, 237.
[55] Z. Zhao, Y. Li, M. Wang, S. Zhao, Z. Zhao, J. Fang, *J. Cell. Mol. Med.* **2020**, *24*, 5408.
[56] J. A. Panadero, S. Lanceros-Mendez, J. L. G. Ribelles, *Acta Biomater.* **2016**, *33*, 1.
[57] A. J. Engler, S. Sen, H. L. Sweeney, D. E. Discher, *Cell* **2006**, *126*, 677.
[58] R. Sunyer, X. Trepat, *Curr. Biol.* **2020**, *30*, R383.
[59] J. A. Espina, C. L. Marchant, E. H. Barriga, *FEBS J.* **2022**, *289*, 2736.
[60] A. Nicolas, A. Besser, S. A. Safran, *Biophys. J.* **2008**, *95*, 527.
[61] M. Whang, J. Kim, *Tissue Eng. Regener. Med.* **2016**, *13*, 126.
[62] L. G. Vincent, Y. S. Choi, B. Alonso-Latorre, J. C. Del Álamo, A. J. Engler, *Biotechnol. J.* **2013**, *8*, 472.
[63] M. Raab, J. Swift, P. C. D. P. Dingal, P. Shah, J.-W. Shin, D. E. Discher, *J. Cell Biol.* **2012**, *199*, 669.
[64] J. R. Tse, A. J. Engler, *PLoS One* **2011**, *6*, e15978.
[65] Z. Li, Y. Gong, S. Sun, Y. Du, D. Lü, X. Liu, M. Long, *Biomaterials* **2013**, *34*, 7616.
[66] R. Olivares-Navarrete, E. M. Lee, K. Smith, S. L. Hyzy, M. Doroudi, J. K. Williams, K. Gall, B. D. Boyan, Z. Schwartz, *PLoS One* **2017**, *12*, e0170312.
[67] W. J. Hadden, J. L. Young, A. W. Holle, M. L. Mcfetridge, D. Y Kim, P. Wijesinghe, H. Taylor-Weiner, J. H. Wen, A. R. Lee, K. Bieback, B.-N. Vo, D. D. Sampson, B. F. Kennedy, J. P. Spatz, A. J. Engler, Y. S. Choi, *Proc. Natl. Acad. Sci. U. S. A.* **2017**, *114*, 5647.
[68] O. Chaudhuri, J. Cooper-White, P. A. Janmey, D. J. Mooney, V. B. Shenoy, *Nature* **2020**, *584*, 535.
[69] R. Mohindra, D. K. Agrawal, F. G. Thankam, *J. Cardiovasc. Transl. Res.* **2021**, *14*, 647.
[70] N. Alcorta-Sevillano, I. Macías, A. Infante, C. I. Rodríguez, *Cells* **2020**, *9*, 2630.
[71] F. Spill, D. S. Reynolds, R. D. Kamm, M. H. Zaman, *Curr. Opin. Biotechnol.* **2016**, *40*, 41.
[72] G. R. Ramirez-San Juan, P. W. Oakes, M. L. Gardel, *Mol. Biol. Cell* **2017**, *28*, 1043.
[73] R. J. Petrie, A. D. Doyle, K. M. Yamada, *Nat. Rev. Mol. Cell Biol.* **2009**, *10*, 538.
[74] S. A. Biela, Y. Su, J. P. Spatz, R. Kemkemer, *Acta Biomater.* **2009**, *5*, 2460.
[75] R. B. Dickinson, S. Guido, R. T. Tranquillo, *Ann. Biomed. Eng.* **1994**, *22*, 342.
[76] S. Gerecht, C. J. Bettinger, Z. Zhang, J. T. Borenstein, G. Vunjak-Novakovic, R. Langer, *Biomaterials* **2007**, *28*, 4068.
[77] A. I. Teixeira, G. A. Abrams, P. J. Bertics, C. J. Murphy, P. F. Nealey, *J. Cell Sci.* **2003**, *116*, 1881.

[78] M. Akhmanova, E. Osidak, S. Domogatsky, S. Rodin, A. Domogatskaya, *Stem Cells Int.* **2015**, *2015*, 167025.
[79] T. Khamdaeng, J. Luo, J. Vappou, P. Terdtoon, E. E. Konofagou, *Ultrasonics* **2012**, *52*, 402.
[80] T. Kietzmann, *Redox Biol.* **2017**, *11*, 622.
[81] M. F. Berry, A. J. Engler, Y. J Woo, T. J. Pirolli, L. T. Bish, V. Jayasankar, K. J. Morine, T. J. Gardner, D. E. Discher, H. L Sweeney, *Am. J. Physiol.: Heart Circ. Physiol.* **2006**, *290*, H2196.
[82] R. Levato, T. Jungst, R. G. Scheuring, T. Blunk, J. Groll, J. Malda, *Adv. Mater.* **2020**, *32*, 1906423.
[83] C. Vasile, D. Pamfil, E. Stoleru, M. Baican, *Molecules* **2020**, *25*, 1539.
[84] K. M. Pryse, A. Nekouzadeh, G. M. Genin, E. L. Elson, G. I. Zahalak, *Ann. Biomed. Eng.* **2003**, *31*, 1287.
[85] T. E. Brown, K. S. Anseth, *Chem. Soc. Rev.* **2017**, *46*, 6532.
[86] E. J. Bolívar-Monsalve, M. M. Alvarez, S. Hosseini, M. A. Espinosa-Hernandez, C. F. Ceballos-González, M. Sanchez-Dominguez, S. R Shin, B. Cecen, S. Hassan, E. Di Maio, G. Trujillo-De Santiago, *Mater. Adv.* **2021**, *2*, 4447.
[87] K. S. Lim, M. H. Alves, L. A. Poole-Warren, P. J. Martens, *Biomaterials* **2013**, *34*, 7097.
[88] D. Barros, P. Parreira, J. Furtado, F. Ferreira-Da-Silva, E. Conde-Sousa, A. J. García, M. C. L. Martins, I. F. Amaral, A. P. Pêgo, *Biomaterials* **2019**, *192*, 601.
[89] J. Jia, R. C. Coyle, D. J. Richards, C. L. Berry, R. W. Barrs, J. Biggs, C. James Chou, T. C. Trusk, Y. Mei, *Acta Biomater.* **2016**, *45*, 110.
[90] W. Lan, M. Xu, M. Qin, Y. Cheng, Y. Zhao, D. Huang, X. Wei, Y. Guo, W. Chen, *Mater. Des.* **2021**, *204*, 109652.
[91] A. Chyzy, M. E. Plonska-Brzezinska, *Molecules* **2020**, *25*, 5795.
[92] K. A. Kyburz, K. S. Anseth, *Acta Biomater.* **2013**, *9*, 6381.
[93] L. Bian, C. Hou, E. Tous, R. Rai, R. L. Mauck, J. A. Burdick, *Biomaterials* **2013**, *34*, 413.
[94] M. J. Webber, E. A. Appel, E. W. Meijer, R. Langer, *Nat. Mater.* **2016**, *15*, 13.
[95] F. L. C. Morgan, L. Moroni, M. B. Baker, *Adv. Healthcare Mater.* **2020**, *9*, 1901798.
[96] W. Sun, D. A. Gregory, X. Zhao, *Adv. Colloid Interface Sci.* **2023**, *314*, 102866.
[97] E. Beniash, J. D. Hartgerink, H. Storrie, J. C. Stendahl, S. I. Stupp, *Acta Biomater.* **2005**, *1*, 387.
[98] J. C. Stendahl, M. S. Rao, M. O. Guler, S. I. Stupp, *Adv. Funct. Mater.* **2006**, *16*, 499.
[99] J. M. Godbe, R. Freeman, L. F. Burbulla, J. Lewis, D. Krainc, S. I. Stupp, *ACS Biomater. Sci. Eng.* **2020**, *6*, 1196.
[100] A. K. Varanko, J. C. Su, A. Chilkoti, *Annu. Rev. Biomed. Eng.* **2020**, *22*, 343.
[101] C. M. Madl, B. L. Lesavage, R. E. Dewi, C. B. Dinh, R. S. Stowers, M. Khariton, K. J. Lampe, D. Nguyen, O. Chaudhuri, A. Enejder, S. C. Heilshorn, *Nat. Mater.* **2017**, *16*, 1233.
[102] D. Zhu, H. Wang, P. Trinh, S. C. Heilshorn, F. Yang, *Biomaterials* **2017**, *127*, 132.
[103] J. Berger, M. Reist, J. M. Mayer, O. Felt, N. A. Peppas, R. Gurny, *Eur. J. Pharm. Biopharm.* **2004**, *57*, 19.
[104] H. Cui, X. Zhuang, C. He, Y. Wei, X. Chen, *Acta Biomater.* **2015**, *11*, 183.
[105] Y. Hu, Z. Zhang, Y. Li, X. Ding, D. Li, C. Shen, F.-J. Xu, *Macromol. Rapid Commun.* **2018**, *39*, 1800069.
[106] C. D. Spicer, *Polym. Chem.* **2020**, *11*, 184.
[107] T. Freier, H. S. Koh, K. Kazazian, M. S. Shoichet, *Biomaterials* **2005**, *26*, 5872.
[108] L. Rami, S. Malaise, S. Delmond, J.-C. Fricain, R. Siadous, S. Schlaubitz, E. Laurichesse, J. Amédée, A. Montembault, L. David, L. Bordenave, *J. Biomed. Mater. Res., Part A* **2014**, *102*, 3666.
[109] O. Chaudhuri, L. Gu, D. Klumpers, M. Darnell, S. A. Bencherif, J. C. Weaver, N. Huebsch, H.-P. Lee, E. Lippens, G. N. Duda, D. J. Mooney, *Nat. Mater.* **2016**, *15*, 326.
[110] L. Q. Wan, J. Jiang, D. E. Arnold, X. E Guo, H. H. Lu, V. C. Mow, *Cell Mol. Bioeng.* **2008**, *1*, 93.
[111] C. B. Rodell, J. E. Mealy, J. A. Burdick, *Bioconjug. Chem.* **2015**, *26*, 2279.
[112] S. M. Mantooth, B. G. Munoz-Robles, M. J. Webber, *Macromol. Biosci.* **2019**, *19*, 1800281.
[113] A. J. Feliciano, C. Van Blitterswijk, L. Moroni, M. B. Baker, *Acta Biomater.* **2021**, *124*, 1.
[114] E. A. Appel, R. A. Forster, A. Koutsioubas, C. Toprakcioglu, O. A. Scherman, *Angew. Chem., Int. Ed.* **2014**, *53*, 10038.
[115] H. W. Ooi, J. M. M. Kocken, F. L. C. Morgan, A. Malheiro, B. Zoetebier, M. Karperien, P. A. Wieringa, P. J. Dijkstra, L. Moroni, M. B. Baker, *Biomacromolecules* **2020**, *21*, 2208.
[116] J. Zhu, R. E. Marchant, *Expert Rev. Med. Devices* **2011**, *8*, 607.
[117] X. Xue, Y. Hu, S. Wang, X. Chen, Y. Jiang, J. Su, *Bioact. Mater.* **2022**, *12*, 327.
[118] B. J. Klotz, D. Gawlitta, A. J. W. P. Rosenberg, J. Malda, F. P. W. Melchels, *Trends Biotechnol.* **2016**, *34*, 394.
[119] B. G. Soliman, G. C. J. Lindberg, T. Jungst, G. J. Hooper, J. Groll, T. B. F. Woodfield, K. S. Lim, *Adv. Healthcare Mater.* **2020**, *9*, 1901544.
[120] S. Bertlein, G. Brown, K. S. Lim, T. Jungst, T. Boeck, T. Blunk, J. Tessmar, G. J. Hooper, T. B. F. Woodfield, J. Groll, *Adv. Mater.* **2017**, *29*, 1703404.
[121] J. Shao, Y. Huang, Q. Fan, *Polym. Chem.* **2014**, *5*, 4195.
[122] W. Tomal, J. Ortyl, *Polymers* **2020**, *12*, 1073.
[123] C. E. Hoyle, C. N. Bowman, *Angew. Chem., Int. Ed. Engl.* **2010**, *49*, 1540.
[124] K. Vats, G. Marsh, K. Harding, I. Zampetakis, R. E. Waugh, D. S. W. Benoit, *J. Biomed. Mater. Res., Part A* **2017**, *105*, 1112.
[125] Y. Han, Y. Cao, H. Lei, *Gels* **2022**, *8*, 577.
[126] S. Hafeez, H. W. Ooi, F. L. C. Morgan, C. Mota, M. Dettin, C. Van Blitterswijk, L. Moroni, M. B. Baker, *Gels* **2018**, *4*, 85.
[127] D. K. Kölmel, E. T. Kool, *Chem. Rev.* **2017**, *117*, 10358.
[128] T. Luo, B. Tan, L. Zhu, Y. Wang, J. Liao, *Front. Bioeng. Biotechnol.* **2022**, *10*, 817391.
[129] M. Ozeki, Y. Tabata, *J. Biomater. Sci., Polym. Ed.* **2005**, *16*, 549.
[130] P. Atienza-Roca, D. C. Kieser, X. Cui, B. Bathish, Y. Ramaswamy, G. J. Hooper, A. N. Clarkson, J. Rnjak-Kovacina, P. J. Martens, L. M. Wise, T. B. F. Woodfield, K. S. Lim, *Biomater. Sci.* **2020**, *8*, 5005.
[131] Elham Badali, M. Hosseini, M. Mohajer, S. Hassanzadeh, S. Saghati, J. Hilborn, M. Khanmohammadi, *Polym. Sci., Ser. A* **2021**, *63*, S1.
[132] Y. Zhang, Y. Cao, H. Zhao, L. Zhang, T. Ni, Y. Liu, Z. An, M. Liu, R. Pei, *J. Mater. Chem. B* **2020**, *8*, 4237.
[133] F. Anjum, P. S. Lienemann, S. Metzger, J. Biernaskie, M. S. Kallos, M. Ehrbar, *Biomaterials* **2016**, *87*, 104.
[134] L. G. Poole, A. K. Kopec, D. J. Groeneveld, A. Pant, K. S. Baker, H. M. Cline-Fedewa, M. J. Flick, J. P. Luyendyk, *Blood* **2021**, *137*, 2520.
[135] T. A. E. Ahmed, E. V. Dare, M. Hincke, *Tissue Eng., Part B* **2008**, *14*, 199.
[136] J. R. Choi, K. W. Yong, J. Y. Choi, A. C. Cowie, *BioTechniques* **2019**, *66*, 40.
[137] E. M. Ahmed, *J. Adv. Res.* **2015**, *6*, 105.
[138] S. J. Bryant, C. R. Nuttelman, K. S. Anseth, *J. Biomater. Sci., Polym. Ed.* **2000**, *11*, 439.
[139] W. Tomal, M. Pilch, A. Chachaj-Brekiesz, M. Galek, F. Morlet-Savary, B. Graff, C. Dietlin, J. Lalevée, J. Ortyl, *Polym. Chem.* **2020**, *11*, 4604.
[140] C. G. Williams, A. N. Malik, T. K. Kim, P. N. Manson, J. H. Elisseeff, *Biomaterials* **2005**, *26*, 1211.
[141] B. D. Fairbanks, M. P. Schwartz, C. N. Bowman, K. S. Anseth, *Biomaterials* **2009**, *30*, 6702.
[142] E. A. Kamoun, A. Winkel, M. Eisenburger, H. Menzel, *Arabian J. Chem.* **2016**, *9*, 745.
[143] H. Shih, C.-C. Lin, *Macromol. Rapid Commun.* **2013**, *34*, 269.

[144] K. S. Lim, B. S. Schon, N. V. Mekhileri, G. C. J. Brown, C. M. Chia, S. Prabakar, G. J. Hooper, T. B. F. Woodfield, *ACS Biomater. Sci. Eng.* **2016**, *2*, 1752.
[145] C. Imberti, P. Zhang, H. Huang, P. J. Sadler, *Angew. Chem., Int. Ed.* **2020**, *59*, 61.
[146] R. Lavker, K. Kaidbey, *J. Invest. Dermatol.* **1997**, *108*, 17.
[147] G. C. J. Lindberg, K. S. Lim, B. G. Soliman, A. Nguyen, G. J. Hooper, R. J. Narayan, T. B. F. Woodfield, *Appl. Phys. Rev.* **2021**, *8*, 011301.
[148] C. Ash, M. Dubec, K. Donne, T. Bashford, *Lasers Med. Sci.* **2017**, *32*, 1909.
[149] J. Elisseeff, K. Anseth, D. Sims, W. Mcintosh, M. Randolph, R. Langer, *Proc. Natl. Acad. Sci. U. S. A.* **1999**, *96*, 3104.
[150] R.-Z. Lin, Y.-C. Chen, R. Moreno-Luna, A. Khademhosseini, J. M. Melero-Martin, *Biomaterials* **2013**, *34*, 6785.
[151] K. S. Lim, B. J. Klotz, G. C. J. Lindberg, F. P. W. Melchels, G. J. Hooper, J. Malda, D. Gawlitta, T. B. F. Woodfield, *Macromol. Biosci.* **2019**, *19*, e1900098.
[152] S. P. B. Teixeira, R. M. A. Domingues, M. Shevchuk, M. E. Gomes, N. A. Peppas, R. L. Reis, *Adv. Funct. Mater.* **2020**, *30*, 1909011.
[153] M. Ehrbar, A. Sala, P. Lienemann, A. Ranga, K. Mosiewicz, A. Bittermann, S. C. Rizzi, F. E. Weber, M. P. Lutolf, *Biophys. J.* **2011**, *100*, 284.
[154] S. Kim, Z.-K. Cui, J. Fan, A. Fartash, T. L. Aghaloo, M. Lee, *J. Mater. Chem. B* **2016**, *4*, 5289.
[155] G. Pitarresi, F. S. Palumbo, C. Fiorica, F. Bongiovì, A. Martorana, S. Federico, C. M. Chinnici, G. Giammona, *Macromol. Biosci.* **2022**, *22*, 2100290.
[156] M. Kumar, P. Gupta, S. Bhattacharjee, S. K. Nandi, B. B. Mandal, *Biomaterials* **2018**, *187*, 1.
[157] L. M. Caballero Aguilar, S. M. Silva, S. E. Moulton, *J. Controlled Release* **2019**, *306*, 40.
[158] A. H. Nguyen, J. Mckinney, T. Miller, T. Bongiorno, T. C. Mcdevitt, *Acta Biomater.* **2015**, *13*, 101.
[159] T. Buie, J. Mccune, E. Cosgriff-Hernandez, *Trends Biotechnol.* **2020**, *38*, 546.
[160] J. Su, S. C. Satchell, J. A. Wertheim, R. N. Shah, *Biomaterials* **2019**, *201*, 99.
[161] K. S. Masters, *Macromol. Biosci.* **2011**, *11*, 1149.
[162] B. V. Sridhar, N. R. Doyle, M. A. Randolph, K. S. Anseth, *J. Biomed. Mater. Res., Part A* **2014**, *102*, 4464.
[163] X. Hu, K. G. Neoh, J. Zhang, E.-T. Kang, W. Wang, *Biomaterials* **2012**, *33*, 8082.
[164] L. L. Y. Chiu, R. D. Weisel, R.-K. Li, M. Radisic, *J. Tissue Eng. Regener. Med.* **2011**, *5*, 69.
[165] B. K. Mann, R. H. Schmedlen, J. L. West, *Biomaterials* **2001**, *22*, 439.
[166] D. L. Mooradian, R. C. Lucas, J. A. Weatherbee, L. T. Furcht, *J. Cell. Biochem.* **1989**, *41*, 189.
[167] B. Wang, P. J. Díaz-Payno, D. C. Browe, F. E. Freeman, J. Nulty, R. Burdis, D. J. Kelly, *Acta Biomater.* **2021**, *128*, 130.
[168] M. H. Hettiaratchi, L. Krishnan, T. Rouse, C. Chou, T. C. Mcdevitt, R. E. Guldberg, *Sci. Adv.* **2020**, *6*, 1240.
[169] Z.-Y. Guan, C.-Y. Wu, J.-T. Wu, C.-H. Tai, J. Yu, H.-Y. Chen, *ACS Appl. Mater. Interfaces* **2016**, *8*, 13812.
[170] K. M. Park, S. Gerecht, *Nat. Commun.* **2014**, *5*, 4075.
[171] X. Wu, W. Huang, W.-H. Wu, B. Xue, D. Xiang, Y. Li, M. Qin, F. Sun, W. Wang, W.-B. Zhang, Y. Cao, *Nano Res.* **2018**, *11*, 5556.
[172] P. Atallah, L. Schirmer, M. Tsurkan, Y. D. Putra Limasale, R. Zimmermann, C. Werner, U. Freudenberg, *Biomaterials* **2018**, *181*, 227.
[173] P. S. Lienemann, Q. Vallmajo-Martin, P. Papageorgiou, U. Blache, S. Metzger, A.-S. Kiveliö, V. Milleret, A. Sala, S. Hoehnel, A. Roch, R. Reuten, M. Koch, O. Naveiras, F. E. Weber, W. Weber, M. P. Lutolf, M. Ehrbar, *Adv. Sci. (Weinheim, Ger.)* **2020**, *7*, 1903395.
[174] K. M. Park, M. R. Blatchley, S. Gerecht, *Macromol. Rapid Commun.* **2014**, *35*, 1968.
[175] D. M. Lewis, M. R. Blatchley, K. M. Park, S. Gerecht, *Nat. Protoc.* **2017**, *12*, 1620.
[176] S. Tan, J. Y. Fang, Z. Yang, M. E. Nimni, B. Han, *Biomaterials* **2014**, *35*, 5294.
[177] R. S. Stowers, S. C. Allen, L. J. Suggs, *Proc. Natl. Acad. Sci. U. S. A.* **2015**, *112*, 1953.
[178] R. K. Das, V. Gocheva, R. Hammink, O. F. Zouani, A. E. Rowan, *Nat. Mater.* **2016**, *15*, 318.
[179] J. H. Wen, L. G. Vincent, A. Fuhrmann, Y. S. Choi, K. C. Hribar, H. Taylor-Weiner, S. Chen, A. J. Engler, *Nat. Mater.* **2014**, *13*, 979.
[180] Y. Ren, H. Zhang, Y. Wang, B. Du, J. Yang, L. Liu, Q. Zhang, *ACS Appl. Bio Mater.* **2021**, *4*, 2601.
[181] Y. S. Choi, L. G. Vincent, A. R. Lee, M. K. Dobke, A. J. Engler, *Biomaterials* **2012**, *33*, 2482.
[182] R. Sunyer, A. J. Jin, R. Nossal, D. L. Sackett, *PLoS One* **2012**, *7*, e46107.
[183] T. Kawano, S. Kidoaki, *Biomaterials* **2011**, *32*, 2725.
[184] B. Wang, J. Shi, J. Wei, X. Tu, Y. Chen, *Biofabrication* **2019**, *11*, 045003.
[185] E. Hadjipanayi, V. Mudera, R. A. Brown, *Cell Motil. Cytoskeleton* **2009**, *66*, 121.
[186] O. Chaudhuri, L. Gu, M. Darnell, D. Klumpers, S. A. Bencherif, J. C. Weaver, N. Huebsch, D. J. Mooney, *Nat. Commun.* **2015**, *6*, 6364.
[187] C. Rieu, C. Parisi, G. Mosser, B. Haye, T. Coradin, F. M. Fernandes, L. Trichet, *ACS Appl. Mater. Interfaces* **2019**, *11*, 14672.
[188] C. D. Hartman, B. C. Isenberg, S. G. Chua, J. Y. Wong, *Proc. Natl. Acad. Sci. U. S. A.* **2016**, *113*, 11190.
[189] G. De Vicente, M. C. Lensen, *Eur. Polym. J.* **2016**, *78*, 290.
[190] S. L. Vega, M. Y. Kwon, K. H. Song, C. Wang, R. L. Mauck, L. Han, J. A. Burdick, *Nat. Commun.* **2018**, *9*, 614.
[191] X. Tong, J. Jiang, D. Zhu, F. Yang, *ACS Biomater. Sci. Eng.* **2016**, *2*, 845.
[192] H. Ravanbakhsh, V. Karamzadeh, G. Bao, L. Mongeau, D. Juncker, Y. S. Zhang, *Adv. Mater.* **2021**, *33*, 2104730.
[193] J. Li, C. Wu, P. K. Chu, M. Gelinsky, *Mater. Sci. Eng.: R: Rep.* **2020**, *140*, 100543.
[194] M. Lee, R. Rizzo, F. Surman, M. Zenobi-Wong, *Chem. Rev.* **2020**, *120*, 10950.
[195] E. L. Gill, X. Li, M. A. Birch, Y. Y. S. Huang, *Bio-Des. Manuf.* **2018**, *1*, 77.
[196] A. Motealleh, B. Çelebi-Saltik, N. Ermis, S. Nowak, A. Khademhosseini, N. S. Kehr, *Biofabrication* **2019**, *11*, 045015.
[197] B. Byambaa, N. Annabi, K. Yue, G. Trujillo-de Santiago, M. M. Alvarez, W. Jia, M. Kazemzadeh-Narbat, S. R. Shin, A. Tamayol, A. Khademhosseini, *Adv. Healthcare Mater.* **2017**, *6*, 1700015.
[198] F. E. Freeman, P. Pitacco, L. H. A. Van Dommelen, J. Nulty, D. C. Browe, J.-Y. Shin, E. Alsberg, D. J. Kelly, *Sci. Adv.*, *6*, 5093.
[199] W. Kim, C. H. Jang, G. Kim, *Theranostics* **2022**, *12*, 5404.
[200] R. L. Truby, J. A. Lewis, *Nature* **2016**, *540*, 371.
[201] J. Malda, J. Visser, F. P. Melchels, T. Jüngst, W. E. Hennink, W. J. A. Dhert, J. Groll, D. W. Hutmacher, *Adv. Mater.* **2013**, *25*, 5011.
[202] K. S. Lim, B. S. Schon, N. V. Mekhileri, G. C. J. Brown, C. M. Chia, S. Prabakar, G. J. Hooper, T. B. F. Woodfield, *ACS Biomater. Sci. Eng.* **2016**, *2*, 1752.
[203] V. H. M. Mouser, F. P. W. Melchels, J. Visser, W. J. A. Dhert, D. Gawlitta, J. Malda, *Biofabrication* **2016**, *8*, 035003.
[204] G. Cidonio, C. R. Alcala-Orozco, K. S. Lim, M. Glinka, I. Mutreja, Y.-H. Kim, J. I. Dawson, T. B. F. Woodfield, R. O. C. Oreffo, *Biofabrication* **2019**, *11*, 035027.
[205] E. A. Guzzi, G. Bovone, M. W. Tibbitt, *Small* **2019**, *15*, 1905421.
[206] L. Ouyang, C. B. Highley, W. Sun, J. A. Burdick, *Adv. Mater.* **2017**, *29*, 1604983.

[207] D. Petta, A. R. Armiento, D. Grijpma, M. Alini, D. Eglin, M. D'este, *Biofabrication* **2018**, *10*, 044104.
[208] T. J. Hinton, Q. Jallerat, R. N. Palchesko, J. H. Park, M. S. Grodzicki, H.-J. Shue, M. H. Ramadan, A. R. Hudson, A. W. Feinberg, *Sci. Adv.* **2015**, *1*, e1500758.
[209] C. B. Highley, K. H. Song, A. C. Daly, J. A. Burdick, *Adv. Sci. (Weinheim, Ger.)* **2019**, *6*, 1801076.
[210] K. S. Lim, M. Baptista, S. Moon, T. B. F. Woodfield, J. Rnjak-Kovacina, *Trends Biotechnol.* **2019**, *37*, 1189.
[211] A. C. Hernández-González, L. Téllez-Jurado, L. M. Rodríguez-Lorenzo, *Carbohydr. Polym.* **2020**, *229*, 115514.
[212] F. E. Freeman, D. J. Kelly, *Sci. Rep.* **2017**, *7*, 17042.
[213] M. D. Giuseppe, N. Law, B. Webb, R. A. Macrae, L. J. Liew, T. B. Sercombe, R. J. Dilley, B. J. Doyle, *J. Mech. Behav. Biomed. Mater.* **2018**, *79*, 150.
[214] G. Janarthanan, J. H. Kim, I. Kim, C. Lee, E. J. Chung, I. Noh, *Biofabrication* **2022**, *14*, 035013.
[215] L. L. Wang, C. B. Highley, Y.-C. Yeh, J. H. Galarraga, S. Uman, J. A. Burdick, *J. Biomed. Mater. Res., Part A* **2018**, *106*, 865.
[216] L. Ouyang, C. B. Highley, C. B. Rodell, W. Sun, J. A. Burdick, *ACS Biomater. Sci. Eng.* **2016**, *2*, 1743.
[217] T. Hu, X. Cui, M. Zhu, M. Wu, Y. Tian, B. Yao, W. Song, Z. Niu, S. Huang, X. Fu, *Bioact. Mater.* **2020**, *5*, 808.
[218] C. Loebel, C. B. Rodell, M. H. Chen, J. A. Burdick, *Nat. Protoc.* **2017**, *12*, 1521.
[219] C. Li, A. Faulkner-Jones, A. R. Dun, J. Jin, P. Chen, Y. Xing, Z. Yang, Z. Li, W. Shu, D. Liu, R. R. Duncan, *Angew. Chem., Int. Ed.* **2015**, *54*, 3957.
[220] C. Cofiño, S. Perez-Amodio, C. E. Semino, E. Engel, M. A. Mateos-Timoneda, *Macromol. Mater. Eng.* **2019**, *304*, 1900353.
[221] R. J. Mondschein, A. Kanitkar, C. B. Williams, S. S. Verbridge, T. E. Long, *Biomaterials* **2017**, *140*, 170.
[222] S. You, P. Wang, J. Schimelman, H. H. Hwang, S. Chen, *Addit. Manuf.* **2019**, *30*, 100834.
[223] N. He, X. Wang, L. Shi, J. Li, L. Mo, F. Chen, Y. Huang, H. Liu, X. Zhu, W. Zhu, Y. Mao, X. Han, *Nat. Commun.* **2023**, *14*, 3063.
[224] B. Grigoryan, S. J. Paulsen, D. C. Corbett, D. W. Sazer, C. L. Fortin, A. J. Zaita, P. T. Greenfield, N. J. Calafat, J. P. Gounley, A. H. Ta, F. Johansson, A. Randles, J. E. Rosenkrantz, J. D. Louis-Rosenberg, P. A. Galie, K. R. Stevens, J. S. Miller, *Science* **2019**, *364*, 458.
[225] J. Huh, Y. W. Moon, J. Park, A. Atala, J. J. Yoo, S. J. Lee, *Biofabrication* **2021**, *13*, 0341030.
[226] K. S. Lim, R. Levato, P. F. Costa, M. D. Castilho, C. R. Alcala-Orozco, K. M. A. Van Dorenmalen, F. P. W. Melchels, D. Gawlitta, G. J. Hooper, J. Malda, T. B. F. Woodfield, *Biofabrication* **2018**, *10*, 034101.
[227] X. Ma, X. Qu, W. Zhu, Y.-S. Li, S. Yuan, H. Zhang, J. Liu, P. Wang, C. S. E. Lai, F. Zanella, G.-S. Feng, F. Sheikh, S. Chien, S. Chen, *Proc. Natl. Acad. Sci. U. S. A.* **2016**, *113*, 2206.
[228] W. Zhu, X. Qu, J. Zhu, X. Ma, S. Patel, J. Liu, P. Wang, C. S. E. Lai, M. Gou, Y. Xu, K. Zhang, S. Chen, *Biomaterials* **2017**, *124*, 106.
[229] W. L. Ng, J. M. Lee, M. Zhou, Y.-W. Chen, K.-X. A. Lee, W. Y. Yeong, Y.-F. Shen, *Biofabrication* **2020**, *12*, 022001.
[230] H. Lin, D. Zhang, P. G. Alexander, G. Yang, J. Tan, A. W.-M. Cheng, R. S. Tuan, *Biomaterials* **2013**, *34*, 331.
[231] P. N. Bernal, P. Delrot, D. Loterie, Y. Li, J. Malda, C. Moser, R. Levato, *Adv. Mater.* **2019**, *31*, 1904209.
[232] P. N. Bernal, M. Bouwmeester, J. Madrid-Wolff, M. Falandt, S. Florczak, N. G. Rodriguez, Y. Li, G. Größbacher, R.-A. Samsom, M. Van Wolferen, L. J. W. Van Der Laan, P. Delrot, D. Loterie, J. Malda, C. Moser, B. Spee, R. Levato, *Adv. Mater.* **2022**, *34*, 2110054.
[233] R. Rizzo, D. Ruetsche, H. Liu, M. Zenobi-Wong, *Adv. Mater.* **2021**, *33*, 2102900.
[234] M. Falandt, P. N. Bernal, O. Dudaryeva, S. Florczak, G. Größbacher, M. Schweiger, A. Longoni, C. Greant, M. Assunção, O. Nijssen, S. Van Vlierberghe, J. Malda, T. Vermonden, R. Levato, *Adv. Mater. Technol.* **2023**, *8*, 2300026.
[235] M. Nie, S. Takeuchi, *Biofabrication* **2018**, *10*, 044103.
[236] Q. Zhong, H. Ding, B. Gao, Z. He, Z. Gu, *Adv. Mater. Technol.* **2019**, *4*, 1800663.
[237] X. Wang, X. Li, X. Dai, X. Zhang, J. Zhang, T. Xu, Q. Lan, *Colloids Surf., B* **2018**, *171*, 291.
[238] R. Attalla, E. Puersten, N. Jain, P. R. Selvaganapathy, *Biofabrication* **2018**, *11*, 015012.
[239] M. Costantini, S. Testa, P. Mozetic, A. Barbetta, C. Fuoco, E. Fornetti, F. Tamiro, S. Bernardini, J. Jaroszewicz, W. Swieszkowski, M. Trombetta, L. Castagnoli, D. Seliktar, P. Garstecki, G. Cesareni, S. Cannata, A. Rainer, C. Gargioli, *Biomaterials* **2017**, *131*, 98.
[240] D. Kang, G. Ahn, D. Kim, H.-W. Kang, S. Yun, W.-S. Yun, J.-H. Shim, S. Jin, *Biofabrication* **2018**, *10*, 035008.
[241] W. Liu, Y. S. Zhang, M. A. Heinrich, F. De Ferrari, H. L. Jang, S. M. Bakht, M. M. Alvarez, J. Yang, Y. C. Li, G. Trujillo-de Santiago, A. K. Miri, K. Zhu, P. Khoshakhlagh, G. Prakash, H. Cheng, X. Guan, Z. Zhong, J. Ju, G. H. Zhu, X. Jin, S. R. Shin, M. R. Dokmeci, A. Khademhosseini, *Adv. Mater.* **2017**, *29*, 1604630.
[242] C. Chávez-Madero, M. D. De León-Derby, M. Samandari, C. F. Ceballos-González, E. J. Bolívar-Monsalve, C. Mendoza-Buenrostro, S. Holmberg, N. A. Garza-Flores, M. A. Almajhadi, I. González-Gamboa, J. F. Yee-De León, S. O. Martínez-Chapa, C. A. Rodríguez, H. K. Wickramasinghe, M. Madou, D. Dean, A. Khademhosseini, Y. S. Zhang, M. M. Alvarez, G. Trujillo-De Santiago, *Biofabrication* **2020**, *12*, 035023.
[243] G. Trujillo-de Santiago, M. M. Alvarez, M. Samandari, G. Prakash, G. Chandrabhatla, P. I. Rellstab-Sánchez, B. Byambaa, P. Pour Shahid Saeed Abadi, S. Mandla, R. K. Avery, A. Vallejo-Arroyo, A. Nasajpour, N. Annabi, Y. S. Zhang, A. Khademhosseini, *Mater. Horiz.* **2018**, *5*, 813.
[244] T. S. Mohan, P. Datta, S. Nesaei, V. Ozbolat, I. T. Ozbolat, *Prog. Biomed. Eng. (Bristol)* **2022**, *4*, 022003.
[245] M. Costantini, J. Idaszek, K. Szöke, J. Jaroszewicz, M. Dentini, A. Barbetta, J. E. Brinchmann, W. Swieszkowski, *Biofabrication* **2016**, *8*, 035002.
[246] Y. S. Zhang, A. Arneri, S. Bersini, S.-R. Shin, K. Zhu, Z. Goli-Malekabadi, J. Aleman, C. Colosi, F. Busignani, V. Dell'erba, C. Bishop, T. Shupe, D. Demarchi, M. Moretti, M. Rasponi, M. R. Dokmeci, A. Atala, A. Khademhosseini, *Biomaterials* **2016**, *110*, 45.
[247] W. Liu, Z. Zhong, N. Hu, Y. Zhou, L. Maggio, A. K. Miri, A. Fragasso, X. Jin, A. Khademhosseini, Y. S. Zhang, *Biofabrication* **2018**, *10*, 024102.
[248] G. Gao, J. H. Lee, J. Jang, D. H. Lee, J.-S. Kong, B. S. Kim, Y.-J. Choi, W. B. Jang, Y. J. Hong, S.-M. Kwon, D.-W. Cho, *Adv. Funct. Mater.* **2017**, *27*, 1700798.
[249] G. Kim, S. Ahn, Y. Kim, Y. Cho, W. Chun, *J. Mater. Chem.* **2011**, *21*, 6165.
[250] Q. Pi, S. Maharjan, X. Yan, X. Liu, B. Singh, A. M. Van Genderen, F. Robledo-Padilla, R. Parra-Saldivar, N. Hu, W. Jia, C. Xu, J. Kang, S. Hassan, H. Cheng, X. Hou, A. Khademhosseini, Y. S. Zhang, *Adv. Mater.* **2018**, *30*, 1706913.
[251] M. Rocca, A. Fragasso, W. Liu, M. A. Heinrich, Y. S. Zhang, *SLAS Technol.* **2018**, *23*, 154.
[252] L. Shao, Q. Gao, H. Zhao, C. Xie, J. Fu, Z. Liu, M. Xiang, Y. He, *Small* **2018**, *14*, e1802187.
[253] C. Colosi, S. R. Shin, V. Manoharan, S. Massa, M. Costantini, A. Barbetta, M. R. Dokmeci, M. Dentini, A. Khademhosseini, *Adv. Mater.* **2016**, *28*, 677.
[254] L. Shao, Q. Gao, C. Xie, J. Fu, M. Xiang, Y. He, *Adv. Healthcare Mater.* **2019**, *8*, e1900014.

[255] F. Feng, J. He, J. Li, M. Mao, D. Li, *Int. J. Bioprint.* **2019**, *5*, 202.
[256] A. K. Miri, D. Nieto, L. Iglesias, H. Goodarzi Hosseinabadi, S. Maharjan, G. U. Ruiz-Esparza, P. Khoshakhlagh, A. Manbachi, M. R. Dokmeci, S. Chen, S. R. Shin, Y. S. Zhang, A. Khademhosseini, *Adv. Mater.* **2018**, *30*, 1800242.
[257] M. Wang, W. Li, L. S. Mille, T. Ching, Z. Luo, G. Tang, C. E. Garciamendez, A. Lesha, M. Hashimoto, Y. S. Zhang, *Adv. Mater.* **2022**, *34*, 2107038.
[258] H. Chu, W. Yang, L. Sun, S. Cai, R. Yang, W. Liang, H. Yu, L. Liu, *Micromachines* **2020**, *11*, 796.
[259] H. A. Alshahrani, *J. Sci.: Adv. Mater. Devices* **2021**, *6*, 167.
[260] Q. Ge, A. H. Sakhaei, H. Lee, C. K. Dunn, N. X. Fang, M. L. Dunn, *Sci. Rep.* **2016**, *6*, 31110.
[261] J. C. Breger, C. Yoon, R. Xiao, H. R. Kwag, M. O. Wang, J. P. Fisher, T. D. Nguyen, D. H. Gracias, *ACS Appl. Mater. Interfaces* **2015**, *7*, 3398.
[262] A. Sydney Gladman, E. A. Matsumoto, R. G. Nuzzo, L. Mahadevan, J. A. Lewis, *Nat. Mater.* **2016**, *15*, 413.
[263] I. Vasiev, A. I. M. Greer, A. Z. Khokhar, J. Stormonth-Darling, K. E Tanner, N. Gadegaard, *Microelectron. Eng.* **2013**, *108*, 76.
[264] S. Pedron, S. Van Lierop, P. Horstman, R. Penterman, D. J. Broer, E. Peeters, *Adv. Funct. Mater.* **2011**, *21*, 1624.
[265] A. Kirillova, R. Maxson, G. Stoychev, C. T. Gomillion, L. Ionov, *Adv. Mater.* **2017**, *29*, 1703443.
[266] Y. Luo, X. Lin, B. Chen, X. Wei, *Biofabrication* **2019**, *11*, 045019.
[267] K. Lavanya, S. V Chandran, K. Balagangadharan, N. Selvamurugan, *Mater. Sci. Eng., C* **2020**, *111*, 110862.
[268] M. M. C. Bastings, S. Koudstaal, R. E. Kieltyka, Y. Nakano, A. C. H. Pape, D. A. M. Feyen, F. J. Van Slochteren, P. A. Doevendans, J. P. G. Sluijter, E. W. Meijer, S. A. J. Chamuleau, P. Y. W. Dankers, *Adv. Healthcare Mater.* **2014**, *3*, 70.
[269] M. Rizwan, R. Yahya, A. Hassan, M. Yar, A. D. Azzahari, V. Selvanathan, F. Sonsudin, C. N. Abouloula, *Polymers (Basel)* **2017**, *9*, 137.
[270] A. Rogina, A. Ressler, I. Matic, G. Gallego Ferrer, I. Marijanovic, M. Ivankovic, H. Ivankovic, *Carbohydr. Polym.* **2017**, *166*, 173.
[271] L. Peng, H. Zhang, A. Feng, M. Huo, Z. Wang, J. Hu, W. Gao, J. Yuan, *Polym. Chem.* **2015**, *6*, 3652.
[272] K. Uto, J. H. Tsui, C. A. Deforest, D.-H. Kim, *Prog. Polym. Sci.* **2017**, *65*, 53.
[273] Y. H. Tran, M. J. Rasmuson, T. Emrick, J. Klier, S. R. Peyton, *Soft Matter* **2017**, *13*, 9007.
[274] S. Matsumoto, S. Yamaguchi, S. Ueno, H. Komatsu, M. Ikeda, K. Ishizuka, Y. Iko, K. V. Tabata, H. Aoki, S. Ito, H. Noji, I. Hamachi, *Chemistry* **2008**, *14*, 3977.
[275] J. T. Van Herpt, M. C. A. Stuart, W. R. Browne, B. L. Feringa, *Chemistry* **2014**, *20*, 3077.
[276] S. Lee, S. Oh, J. Lee, Y. Malpani, Y.-S. Jung, B. Kang, J. Y. Lee, K. Ozasa, T. Isoshima, S. Y. Lee, M. Hara, D. Hashizume, J.-M. Kim, *Langmuir* **2013**, *29*, 5869.
[277] A. Tabet, R. A. Forster, C. C. Parkins, G. Wu, O. A. Scherman, *Polym. Chem.* **2019**, *10*, 467.
[278] A. M. Kloxin, A. M. Kasko, C. N. Salinas, K. S. Anseth, *Science* **2009**, *324*, 59.
[279] C. A. Deforest, D. A. Tirrell, *Nat. Mater.* **2015**, *14*, 523.
[280] P. E. Farahani, S. M. Adelmund, J. A. Shadish, C. A. Deforest, *J. Mater. Chem. B* **2017**, *5*, 4435.
[281] C. K. Arakawa, B. A. Badeau, Y. Zheng, C. A. DeForest, *Adv. Mater.* **2017**, *29*, 1703156.
[282] J. A. Shadish, G. M. Benuska, C. A. Deforest, *Nat. Mater.* **2019**, *18*, 1005.
[283] S. C Dennis, C. J. Berkland, L. F. Bonewald, M. S. Detamore, *Tissue Eng., Part B* **2015**, *21*, 247.
[284] A. Shellard, R. Mayor, *Dev. Cell* **2021**, *56*, 227.
[285] P. Kolar, T. Gaber, C. Perka, G. N. Duda, F. Buttgereit, *Clin. Orthop. Relat. Res.* **2011**, *469*, 3118.
[286] F. Taraballi, M. Sushnitha, C. Tsao, G. Bauza, C. Liverani, A. Shi, E. Tasciotti, *Adv. Healthcare Mater.* **2018**, *7*, e1800490.
[287] M. Manassero, J. Paquet, M. Deschepper, V. Viateau, J. Retortillo, M. Bensidhoum, D. Logeart-Avramoglou, H. Petite, *Tissue Eng., Part A* **2016**, *22*, 534.
[288] L. P. Frazão, J. Vieira de Castro, C. Nogueira-Silva, N. M. Neves, *Biomolecules* **2020**, *10*, 1208.
[289] M. J. Webber, O. F. Khan, S. A. Sydlik, B. C. Tang, R. Langer, *Ann. Biomed. Eng.* **2015**, *43*, 641.
[290] C. H. Evans, *Tissue Eng., Part B* **2011**, *17*, 437.

Bram Soliman is a Postdoctoral Researcher at the University of New South Wales, Australia. In 2018, he came to New Zealand as a Ph.D. candidate at the University of Otago. Christchurch under the primary supervision of Assoc. Prof. Khoon Lim. He investigated how intelligently designed biomaterials can be used with novel biofabrication techniques to control the macro- and microenvironment physical features of engineered tissue and his work was recognized with the Division of Health Sciences Award for Outstanding Ph.D. Thesis. His research currently focusses on the development of high-throughput in vitro 3D cancer models.

Alessia Longoni currently works as a postdoctoral researcher at the University Medical Center (UMC) Utrecht. She obtained her B.Sc. and M.Sc. in Cellular and Molecular Biotechnology at San Raffaele University in Milan. In 2020, after graduating from UMC Utrecht with a Ph.D. degree, she joined Assoc. Prof. Lim's group at the University of Otago as a postdoctoral researcher. Her research interests include bone and vascular tissue engineering, osteoimmunology, and the development of bone marrow organoids to study hematopoiesis.

Tim B. F. Woodfield is Professor of Regenerative Medicine, Department of Orthopaedic Surgery, University of Otago, New Zealand. His research involves developing advanced bioinks, spheroids bioassemby and additive manufacturing platforms applied to musculoskeletal regenerative medicine. Tim is a Fellow of Biomaterials Science & Engineering and recipient of: Rutherford Discovery Fellowship; Australasian Society for Biomaterials & Tissue Engineering (ASBTE) Research Excellence Award; Otago University Research Gold Medal. Tim is President of International Society for Biofabrication, past ASBTE President and sits on the TERMIS-AP Council.

Khoon S. Lim is currently an Australian Research Council Future Fellow and Associate Professor in the School of Medical Sciences at the University of Sydney. He leads the Light Activated Biomaterials (LAB) Group and his research focuses on developing photopolymerizable hydrogel bioinks for tissue engineering and regenerative medicine applications. He is the current President of the Australasian Society for Biomaterials and Tissue Engineering, as well as serves on the Board of Directors of the International Society for Biofabrication. He sits on Editorial Boards of several journals, including Macromolecular Bioscience, Biofabrication and Biomaterials Science.